HYPK scaffolds the Nedd8 and LC3 proteins to initiate the formation of autophagosome around the poly-neddylated huntingtin exon1 aggregates

Running title: **HYPK delivers the poly-neddylated huntingtin exon1 aggregates to autophagosome**

Debasish Kumar Ghosh[1], Ajit Roy[1] and Akash Ranjan[1,*]

[1]Computational and Functional Genomics Group
Centre for DNA Fingerprinting and Diagnostics
Uppal, Hyderabad 500039, Telangana. INDIA

*Corresponding author

Email: akash@cdfd.org.in
Telephone: +91-40-27216159
Fax: +91-40-27216006

ORCID of Dr. Akash Ranjan: 0000-0002-4582-1553
ORCID of Dr. Debasish Kumar Ghosh: 0000-0002-9196-0685

ABSTRACT

Selective autophagy of protein aggregates is necessary for maintaining the cellular proteostasis. Several regulatory proteins play critical roles in this process. Here, we report that the huntingtin interacting protein K (HYPK) modulates the autophagic degradation of poly-neddylated huntingtin exon1 aggregates. HYPK functions as a scaffolding protein that binds to the Nedd8 and LC3 proteins. The C-terminal ubiquitin-associated (UBA) domain of HYPK binds to the Nedd8, whereas an N-terminal tyrosine-type (Y-type) LC3 interacting region (LIR) of HYPK binds to the LC3. Several conserved amino acids in the UBA domain of HYPK are necessary to mediate the efficient binding of HYPK to Nedd8. The autophagy inducing properties of HYPK are manifested by the increased lipidation of LC3 protein, increased expression of beclin-1 and ATG-5 proteins, and generation of puncta-like granules of LC3 in the HYPK overexpressing cells. Association of the 'H-granules' of HYPK with the poly-neddylated huntingtin exon1 aggregates results in the formation of autophagosome around the huntingtin exon1 aggregates, thereby clearing the aggregates by aggrephagy. Poly-neddylation of huntingtin exon1 is required for its autophagic degradation by HYPK. Thus, overexpression of Nedd8 also increases the basal level of cellular autophagy, other than maintaining the autophagy flux. The poly-neddylation dependent autophagic clearance of huntingtin exon1 by HYPK leads to better cell physiology and survival. Taken together, our study describes a novel mechanism of HYPK mediated autophagy of poly-neddylated huntingtin exon1 aggregates.

KEY WORDS

Autophagy, Poly-neddylation, Huntingtin exon1 aggregates, Sequestration, HYPK

INTRODUCTION

The regulatory mechanisms of proteostasis maintain the quality and quantity of the cellular proteins (**1**). Several regulatory processes function globally to monitor the quality of nascent polypeptides or degrade the nonfunctional proteins (**2**). Chaperones (**3**), unfolded protein response (**4**) and post-translational modifications (**5**) are important components of the proteome-controlling pathways. Specialized processes and machineries are also required to cope up the stress of misfolded and aggregated proteins. These myriads of systems are robust, specific and selective in degrading different forms of proteins (**6**), and they play critical functions in different neurodegenerative diseases that ensue due to intra- or extra-cellular accumulation of toxic protein aggregates (**7**). Proteasomal pathway serves as the major mode of clearance of most of the cellular proteins (**8**). More intricate mechanisms, like autophagy, are also involved in recycling the aberrant forms of proteins (**9**). Protein aggregates can be degraded by selective macro-autophagy which is also termed as aggrephagy (**10**). Poly-ubiquitinated protein aggregates undergo aggrephagy by the help of different autophagic proteins, like SQSTM1, LC3, beclin-1, ATGs etc. (**11**). Various studies have uncovered many details of the aggrephagy process (**12**). As an alternative mechanism of autophagy of the toxic protein aggregates, we describe a unique mechanism of HYPK mediated aggrephagy of poly-neddylated huntingtin exon1.

Post-translational modifications (PTMs) of proteins can be the marking events that direct their degradation by proteasomal or autophagy pathways (**13**). Attachment of ubiquitin and/or ubiquitin-like modifiers (like Nedd8, SUMO1, FAT10 etc.) to proteins are indispensable for their degradation. Although ubiquitination process and its effects are vividly studied in protein degradation pathways, few studies report that the neuronal precursor cell expressed developmentally down-regulated 8 (Nedd8) protein can also functionally complement ubiquitin in protein degradation pathway(s) (**14**). Nedd8 is a ubiquitin-like protein which can be linked to specific substrates to form poly-neddylated proteins (**15**). Activation of Nedd8 is done by its C-terminal cleavage by APPBP1/ UBA3 (**16**). Downstream E2 and E3 ligases covalently attach the processed Nedd8 to its cognate substrate(s) (**17**). Poly-neddylation signals as a degradation signature of proteins in cancer (**18**) and in neurodegenerative disease (**19**).

HYPK is an aggregate-sequestering protein (**20**). It can sequester the aggregates of huntingtin exon1, α-synuclein-A53T and superoxide dismutase 1-G93A. The annular oligomers of HYPK, termed as H-granule, are involved in sequestering the protein aggregates (**20**). The balance of structural convolution of HYPK oligomers arises due to complex intra- and inter-molecular interactions of the hydrophobic regions, low complexity region and disordered nanostructure of HYPK (**21**). HYPK also shows chaperone-like activity (**22**) at ribosome where it interacts with the N-acetyl transferase and eIF1A1 proteins (**23**). Other than its effects in proteostasis, HYPK also regulates the cell cycle by interacting with many cytoplasmic and nuclear proteins (**24**). In *Caenorhabditis elegans*, HYPK forms proteasome blocking complex (**25**), and it regulates the aging of the organism (**26**).

In this study, we describe a novel scaffolding function of HYPK that helps this protein to function as an autophagy modulatory protein. The adaptor function of HYPK brings the poly-neddylated protein aggregates, such as poly-neddylated huntingtin exon1 aggregates, and LC3 together to augment the autophagosome formation around the aggregates of poly-neddylated huntingtin exon1. The UBA

domain and LIR of HYPK help in simultaneous binding of HYPK to Nedd8 and LC3. The H-granules of HYPK play key role in sequestering the poly-neddylated huntingtin exon1 aggregates during the formation of the autophagosome around the aggregates. Overexpression of HYPK and Nedd8 increases and maintains the flux of cellular autophagy. HYPK's function in aggrephagy help in restoring the cell physiology and prevent cell death during protoetoxicity.

RESULTS

HYPK interacts with the Nedd8 protein by its C-terminal ubiquitin-associated domain

HYPK is an aggregate-sequestering protein (**20**). Our earlier study had shown that the aggregate-sequestering function of HYPK is linked to the facilitated degradation of the aggregation-prone proteins (**20**). Since HYPK is a key component of the proteostasis network, we find it tempting to understand how HYPK delivers the sequestered toxic protein aggregates to the degradation system(s).

In the previous study, we had observed that the C-terminal region of HYPK was necessary for sequestering the huntingtin exon1 aggregates (**20**). A computational annotation had shown the existence of a putative UBA domain in the C-terminal region of HYPK. This UBA domain is well conserved in the HYPK proteins of different organisms (**Supporting figure 1A**). The sequence of the HYPK-UBA domain is unique, and it does not show significant sequence similarity with most of the other UBA domains of human proteins. Since UBA domains are known to bind ubiquitin and/or ubiquitin-like proteins, we were interested to find the binding partner of HYPK-UBA. In a sequence alignment-based phylogenetic analysis to cluster the similar UBA domains of human proteins, we found that the sequence of second UBA domain (UBA2) of the Nedd8 ultimate buster 1 (NUB1) protein is closest to the sequence of HYPK-UBA domain (**Supporting figure 1B**). NUB1 protein is known to bind to Nedd8 protein (**27**). NUB1 binding to Nedd8 protein regulates the delivery of poly-neddylated huntingtin aggregates to the proteasome (**28**). Given the sequence similarity of HYPK-UBA and NUB1-UBA2, we tested if Nedd8 is an interacting partner of HYPK-UBA. We found that HYPK could strongly bind to the Nedd8 by its UBA domain. Immunoprecipitation of Nedd8 from IMR-32 cell lysate in non-denaturing condition, followed by immunoblotting experiments showed that both HYPK and HYPK-UBA could be pulled-down with enriched Nedd8 (**Figure 1A**). A reciprocal immunoprecipitation of HYPK from IMR-32 cell extract, followed by immunoblotting for Nedd8 and HYPK was also done to test which form of Nedd8 binds to HYPK. The whole Nedd8 immunoblot profile showed that HYPK could interact with monomeric Nedd8, as well as the Nedd8 of poly-neddylation chain (**Figure 1A**). Immunoprecipitation of Nedd8 or HYPK in non-denaturing condition could indicate that HYPK and HYPK-UBA were either bound to Nedd8 or they were neddylated. We observed that HYPK and HYPK-UBA signals disappeared in denaturing (with 1% SDS) immunoprecipitation of Nedd8 (data not shown), indicating that HYPK and HYPK-UBA were not neddylated, but they were bound to Nedd8. Confocal microscopy images also confirmed the significantly high colocalization of HYPK and HYPK-UBA with the Nedd8 protein in IMR-32 cells (**Figure 1B**).

We identified the critical residues of the HYPK-UBA domain that were required for strong and efficient binding of HYPK to Nedd8 protein. Sequence alignment of the UBA domain of the HYPK proteins of different organisms showed four conserved amino acids: aspartate-94 (D94), glutamate-101 (E101), leucine-113 (L113) and glycine-118 (G118) [residue positions were numbered according to the

human HYPK protein isoform-1; NCBI accession number: NP_057484.3] (**Supporting figure 1A**). We generated different mutants of HYPK-UBA in which the conserved residues were either mutated or deleted (**Figure 1C**). In the HYPK-UBA D94A, E101A construct, the D94 and E101 residues were mutated to alanine. The L113 and G118 residues were deleted in the HYPK-UBA ΔL113, ΔG118 mutant. In the surface plasmon resonance (SPR)-based protein-protein interaction study, both the mutants showed lower binding affinity for Nedd8 compared to the wild type HYPK-UBA (**Figure 1D**). This indicated that the four conserved residues of HYPK-UBA were necessary, but not sufficient, for HYPK-UBA interaction with Nedd8. While the conserved amino acids in HYPK-UBA might be critical for HYPK binding to the Nedd8 protein, the neighboring residues might provide additional support to this interaction. We also observed that the full-length HYPK had lower binding affinity for Nedd8 than its UBA domain (**Figure 1D**). We understand that the partially reduced affinity of HYPK for Nedd8 was due to the interference of HYPK's N-terminus in the interaction. We had previously shown that the N-terminus of HYPK was a disordered nanostructure (**21**). It could bend towards the C-terminus and interact with the C-terminal low complexity region (LCR) of HYPK (**21**). Such an interaction could lower the affinity of UBA of full-length HYPK for Nedd8.

HYPK binds to LC3 by its tyrosine-type LC3 interacting region

In the next section of our study, we endeavored to find more clues on HYPK interactions that could modulate the degradation of aggregation-prone proteins. The HYPK sequence contains a conserved tyrosine residue (Y49 residue in human HYPK protein) in its N-terminal region (**Figure 2A**). Since many proteins are reported to contain tyrosine-type (Y-type) LC3 interacting region (LIR), we tested if the conserved tyrosine of HYPK was also a part of Y-type LIR. Sequence alignment of the HYPK-LIR with the Y-type LIRs of other LC3 interacting proteins showed that the HYPK's Y49 was conserved with the tyrosine residues of other LC3 interacting proteins (**Figure 2A**).

Protein-protein interaction studies by non-denaturing immunoprecipitation of HYPK from IMR-32 cell lysate, followed by immunoblotting experiments had shown that LC3 was an interacting partner of HYPK (**Figure 2B**). This observation was corroborated by the findings of a recent study that also reported HYPK interaction with LC3 (**29**). In order to probe the region and residue(s) of HYPK that could mediate its interaction with LC3, we made several deletion mutant constructs of HYPK (**Figure 2C**). The HYPK-N60 and HYPK-C69 constructs contained the N-terminal sixty amino acids (including the putative Y-type LIR) and C-terminal sixty-nine amino acids respectively. The HYPK-Δ^{48}DYA^{50} was a deletion mutant construct in which the 48th-50th residues (DYA) were deleted in the full-length HYPK. Using isothermal titration calorimetry (ITC)-based experiments, we showed that the full length HYPK and HYPK-N60 were able to bind to the LC3 protein (**Figure 2D**). On the contrary, the HYPK-C69 and HYPK-Δ^{48}DYA^{50} did not bind to LC3 (**Figure 2D**). This validated the fact that the N-terminal Y49 was the critical residue for HYPK interaction with LC3. Since the LIR motif of HYPK lacks the conserved hydrophobic residues (leucine, valine or isoleucine) and has instead glutamic acid at this position, it is possible that the HYPK-LIR binds to LC3 in a non-canonical way. To confirm that HYPK and its LIR definitely binds to LC3, we conducted protein-protein interaction studies by pull-down assays using recombinant proteins. We coexpressed recombinant 6xHistidine tagged HYPK/ HYPK-N60/ HYPK-C69/ HYPK-Δ^{48}DYA^{50} and untagged LC3 in BL21DE3 strain of *Escherichia coli* by using pETDuet-1 vector (pETDuet-1 vector allows simultaneous

coexpression of two recombinant proteins in T7 promoter expression system). While nickel-NTA affinity-based column chromatographic purification of HYPK and HYPK-N60 showed the copurification of LC3, purification of HYPK-C69 and HYPK-Δ^{48}DYA^{50} did not copurify LC3 (**Supporting figure 2A**). We also traced the colocalization of HYPK, HYPK-N60, HYPK-C69 and HYPK-Δ^{48}DYA^{50} with LC3 protein in IMR-32 cells. HYPK and HYPK-N60, but not the HYPK-C69 and HYPK-Δ^{48}DYA^{50}, showed significantly high colocalization with LC3 (**Figure 2E, 2F**). These results verified the fact that HYPK interacts with LC3 by its Y-type LIR. However, it remains to be understood if the HYPK-LIR interacts with the LDS of LC3.

We tested if HYPK binds to all or only a subset of the human LC3 homologues (LC3A, LC3B, GABARAP, GABARAPL1 and GABARAPL2). pETDuet-1 mediated bacterial coexpression of untagged HYPK with 6xHistidine tagged LC3A/ LC3B/ GABARAP/ GABARAPL1/ GABARAPL2 revealed that HYPK could copurify with all the homologues of LC3 (**Supporting figure 2B**), suggesting that HYPK can globally interact with different LC3-like proteins.

HYPK induces autophagy

Having found that HYPK could interact with LC3 and Nedd8, the next relevant question was to find if HYPK had any function in modulating the autophagy process. Our results indicated that HYPK could induce and maintain the autophagy flux in human IMR-32 cells. Overexpression of HYPK was observed to induce autophagy-related events, like enhancing the conversion of LC3 protein from state-I to state-II and upregulated expression of autophagic proteins beclin-1, ATG-5 etc. (**Figure 3A**). To understand if HYPK expression was also involved in maintaining the autophagy flux, we conducted time-chase experiments to monitor the cellular levels of LC3-II, beclin-1 and ATG-5 during overexpression of HYPK. We found that HYPK maintained the steady-state temporal flux of autophagy by continuously stimulating the lipidation of LC3-I and increasing the expression of beclin-1 and ATG-5 (**Figure 3A**). Opposingly, when cellular expression of HYPK was knocked-down by HYPK specific shRNA (HYPK-shRNA), the basal level of LC3-I conversion to LC3-II was reduced (**Figure 3B**). In IMR-32 cells, endogenous HYPK also showed significantly high colocalization with beclin-1, but not with the 26S proteasomal protein PSMD8 (**Figure 3C**). HYPK increased the formation of puncta-like LC3-containing structures in the cells. Using the fluorescence and transmission electron microscopy, we identified higher number of LC3 puncta and autophagosomes in the cells that overexpressed HYPK. HYPK-EGFP showed good colocalization with LC3-mCherry puncta (**Figure 3D**). While it was evident that the count of autophagy vacuoles (AV) were higher in HYPK overexpressing cells, it was also observed that HYPK enhanced the fusion of autophagosome-enclosed substrate(s), like huntingtin-exon1 aggregate, with lysosomes to form autolysosomes (AL) (**Figure 3E**).

HYPK's function in autophagy was Nedd8 dependent. When Nedd8 was depleted from the cells by Nedd8 specific shRNA (Nedd8-shRNA), HYPK's capacity of inducing the autophagy process was compromised (**Figure 3F**). Lower level of cellular Nedd8 decreased the conversion of LC3-I to LC3-II and decreased ATG-5 expression, even in a condition that showed overexpression of HYPK.

We further studied the simultaneous colocalization of HYPK and its domains with Nedd8 and different autophagy-related proteins. HYPK and Nedd8 proteins showed significantly high colocalization

with LC3 and ATG-5 proteins in IMR-32 cells (**Figure 4A, 4C**). Colocalization of Nedd8, HYPK and LC3/ ATG-5 implied that HYPK could act on the poly-neddylated proteins during autophagy. The UBA domain of HYPK colocalized with the Nedd8, but not with the LC3 protein (**Figure 4B upper panel, 4C**). On the contrary, the N-terminal region of HYPK (HYPK-N84 that contained the LIR) colocalized with LC3 (**Figure 4B lower panel, 4C**). HYPK-N84 did not coassociate with Nedd8 (**Figure 4B lower panel**). These results showed that the full-length HYPK protein functions as a tethering protein that link the poly-neddylated proteins to autophagic proteins. Neither of the HYPK's domains could individually augment the autophagy process. This is due to the lack of abilities of HYPK-UBA or HYPK-LIR to simultaneously hold the Nedd8 and LC3 proteins.

HYPK augments the aggrephagy of poly-neddylated huntingtin exon1 aggregates

We identified huntingtin exon1 as the substrates of HYPK mediated autophagic degradation. We followed the degradation of aggregation-prone huntingtin exon1 (Htt97Qexon1) in varying conditions that blocked the proteasomal and/or autophagic degradation of proteins. Degradation of Htt97Qexon1 by HYPK continued even in MG132 mediated proteasome inhibited condition (**Figure 5A**). However, treatment of the cells with autophagy inhibitor (chloroquine) had shown reduction in HYPK's capacity of degrading Htt97Qexon1 (**Figure 5A**), indicating that HYPK functions in the autophagic clearance of Htt97Qexon1. We validated HYPK's role in autophagic degradation of Htt97Qexon1 by knocking-down ATG-5. Knock-down of cellular mRNAs of ATG-5 by ATG-5 specific shRNA (ATG-5-shRNA) led to HYPK's incapability of degrading Htt97Qexon1 (**Figure 5B**).

Autophagic proteins, like LC3, ATG-5, ATG-12 etc., were seen to be deposited around the HYPK-poly-neddylated Htt97Qexon1 aggregates (**Figure 5C, 5D**). We had previously reported that the annular-shaped structures of HYPK, termed as H-granule, were necessary for sequestering the huntingtin exon1 aggregates (**20**). We reasoned that the H-granules were associated with the delivery of Htt97Qexon1 aggregates to autophagosomes. We observed the existence of small puncta-like HYPK granules (i.e. the H-granules) beside the poly-neddylated Htt97Qexon1 aggregates (**Figure 5D**). Such findings prove that the sequestration of poly-neddylated huntingtin exon1 aggregates by the H-granules of HYPK acted as the initiating event of formation of autophagosome around the poly-neddylated Htt97Qexon1 aggregates. We understood that the HYPK-UBA was bound to the Nedd8 moieties of the poly-neddylation chains that were linked to the Htt97Qexon1 protein. The HYPK-LIR attracted the LC3 to the aggresomes. Thus, the scaffolding function of HYPK for Nedd8 and LC3 was necessary for the beginning of formation of autophagosome around the huntingtin exon1 aggregates.

We made efforts to *in vitro* reconstitute the multi-subunit structure of the H-granule-sequestered poly-neddylated Htt97Qexon1 in presence of LC3. The reconstitution of the complex was done by purified (>98% pure) recombinant proteins of Htt97Qexon1, HYPK, Nedd8, and LC3. At first, Nedd8 was cross-linked to Htt97Qexon1 by the DSS cross-linking method, followed by incubation of the cross-linked adduct with equimolar mixture of HYPK and LC3. The scanning electron micrographs showed that the H-granules of HYPK sequestered the neddylated Htt97Qexon1 aggregates (**Figure 5E**). The ternary complex of neddylated-Htt97Qexon1/ HYPK/ LC3 was spherical structure which was conducive for the generation of autophagosome initiation complex (**Figure 5E**).

Poly-neddylated proteins undergo autophagic degradation

The delivery of poly-neddylated huntingtin exon1 aggregates to autophagosome raised the question if poly-neddylated proteins are in general subjected to autophagic degradation. Ectopic overexpression of Nedd8 showed an enhancement of the basal level of cellular autophagy. Conversion of LC3-I to LC3-II and higher levels of beclin-1 and ATG-5 were observed to be associated with the overexpression of Nedd8 in IMR-32 cells (**Figure 6A**). Like HYPK, Nedd8 also maintained the autophagy flux which was observable by time-dependent increase in cellular levels of beclin-1 and ATG-5 and conversion of LC3-I to LC3-II during higher expression of Nedd8 (**Figure 6A**). The number of LC3 puncta was significantly higher in the Nedd8 overexpressing cells than the control cells (**Figure 6B**).

The exon1 of huntingtin protein undergoes poly-neddylation, and the poly-neddylated huntingtin exon1 can be a substrate of autophagic degradation. We noticed that the huntingtin exon1 was poly-neddylated in the overexpressed and in the endogenous expression of Nedd8 (**Figure 7A**). Huntingtin exon1 formed high molecular weight complexes that resembled the Nedd8 conjugated structures of the protein. The immunoprecipitation steps in this, and in following experiments, were carried out in the denaturing condition (in presence of 1% SDS) to purify only the neddylated huntingtin exon1, and not any Nedd8 that could non-covalently associate with the huntingtin exon1. Neddylation of huntingtin exon1 aggregates in IMR-32 cells was also apparent from the observation that showed higher amount of Nedd8 deposition with the Htt97Qexon1 aggregates (**Figure 7B**). Nedd8 deposition with Htt97Qexon1 aggregates was more specific, and not just trapping of Nedd8 with the sticky huntingtin exon1 aggregates. It was evident that Nedd8 deposited with Htt97Qexon1 aggregates, but a nonspecific protein, like blue fluorescent protein (BFP), was not deposited with the aggregates (**Figure 7B**).

The huntingtin exon1 could be, in theory, subjected to three different types of neddylation: mononeddylation, poly-neddylation and multi-mononeddylation. To understand which kind of neddylation occurred to Htt97Qexon1, we generated a Nedd8 mutant construct in which all the lysine residues of Nedd8 were mutated to arginine (Nedd8-allR) (**Supporting figure 3A**). This Nedd8-allR mutant cannot be linked to another Nedd8-allR molecule through lysine-linkage, thereby preventing the formation of poly-neddylated chains consisting of Nedd8-allR. However, Nedd8-allR can be conjugated to proteins to form mononeddylated and/or multi-mononeddylated substrates. Coexpression of Htt97Qexon1 with Nedd8 or Nedd8-allR showed that high molecular weight Nedd8 conjugated complexes of Htt97Qexon1 formed only in presence of Nedd8 (**Supporting figure 3A**). Nedd8-allR conjugation resulted in mononeddylated Htt97Qexon1, but not the poly-neddylation or multi-mononeddylation of Htt97Qexon1. This result determined that Htt97Qexon1 was poly-neddylated, and not multi-mononeddylated.

Overexpression of Nedd8 induces the formation of protein-conjugated Nedd8 chains that are mixed with ubiquitin. This event though does not depend on the Nedd8-activating enzyme (NAE1) but rather Nedd8 is activated by the ubiquitin-activating enzyme (UBA1). We clarified the homogeneous poly-neddylation of Htt97Qexon1 by use of NAE1 and UBA1 inhibitors. Treatment of the Htt97Qexon1 expressing IMR-32 cells with NAE1 inhibitor, MLN4924, had decreased the poly-neddylation of the

298 protein (**Supporting figure 3B**). However, application of UAE1 inhibitor, MLN7243, to the cells had no
299 effects in the poly-neddylation of huntingtin exon1 (**Supporting figure 3B**).

300 Neddylation of huntingtin exon1 had direct effects on its degradation. Overexpression of Nedd8
301 was associated with facilitated degradation of huntingtin exon1 (**Figure 7A**). Proteins are redundantly
302 degraded by proteasomal and autophagy pathways. We found that poly-neddylated proteins can be
303 degraded by autophagy. Inhibition of the 26S proteasome (by MG132) or preventing the fusion of
304 autophagosome and lysosome (by chloroquine) had partially, but not completely, prevented the Nedd8
305 mediated degradation of Htt97Qexon1 (**Figure 7C**). Inhibition of both the proteasomal and autophagy
306 pathways had caused the complete blockade of Htt97Qexon1 degradation (**Figure 7C**). Since Nedd8
307 could enhance the degradation of Htt97Qexon1 even in presence of MG132, we understood that Nedd8
308 had regulatory functions in the autophagic degradation of proteins. When cellular ATG-5 level was
309 lowered by ATG-5 specific shRNA (ATG-5-shRNA) in different Nedd8 expressing and MG132 treated
310 conditions, we noted that Nedd8 could not enhance the degradation of Htt97Qexon1 in the ATG-5
311 knocked-down condition (**Figure 7D**). Overall, these observations proved that Nedd8 is an autophagy
312 modulating protein and poly-neddylation serves as a signal of canonical autophagic degradation of
313 proteins.

314 **HYPK helps in cell survival during proteotoxic stress**

315 We investigated if HYPK had positive effects in cell survival and cell physiology during the
316 proteotoxic stress. HYPK showed aiding functions in maintenance of normal cell physiology, even in
317 presence of toxic huntingtin exon1 aggregates. Huntingtin aggregates were reported to cause
318 proteotoxic stress in mouse neuroblastoma cell (Neuro2a), leading to decreased neurite formation in
319 those cells (**30**). Overexpression of HYPK reduced the proteotoxic stress of Htt97Qexon1 aggregates and
320 reinitiated the normal neurite formation in Neuro2a cells (**Figure 8A**).

321 HYPK also helps in survival of cells during the presence of proteotoxicity. Expression of
322 Htt97Qexon1 has lethal effects in terms of perturbing the cell cycle and causing death of IMR-32 cells.
323 Other than reducing the death, overexpression of HYPK also restored the normal cell cycle of
324 Htt97Qexon1 expressing IMR-32 cells (**Figure 8B**). We speculate that the HYPK mediated autophagic
325 degradation of poly-neddylated Htt97Qexon1 aggregates is responsible for the better cell survival.

326 Information derived from gene expression omnibus (GEO) showed that the HYPK expression was
327 not significantly changed in different neurodegenerative disorders/ brain related diseases and in cellular
328 stresses (**Figure 8C, Supporting table 1, 2**). This makes HYPK a potential target that can be modulated to
329 deal with the protein aggregate in neurodegenerative diseases. Many of the HYPK interacting proteins
330 contain one or more aggregation-prone regions (**Figure 8D**). We hypothesize that HYPK interaction with
331 them was a part of cellular surveillance system that monitor cellular proteostasis.

332 Finally, the relevance of protein neddylation in Huntington's disease (HD) can be interpreted by
333 following some of the previous studies (**31, 32, 33**). The GEO profiles of Huntington's disease (Q111)
334 knock-in model in mouse embryonic stem cells (GEO: GDS4533) (**31**) and striatum (GEO: GDS4534) (**32**)
335 showed that the expression of Nedd8 transcript was significantly less in HD mice than control mice

(**Figure 8E**). The expression of NUB1 was also significantly decreased in 27 weeks aged HD transgenic mice (GEO: GDS2912) (**32**) compared to normal mice (**Figure 8E**). However, the expression of the Nedd8 activating enzyme (NAE1) did not alter significantly in HD compared to normal mice (GEO: GDS2912) (**33**) (**Figure 8E**). These results indicate that the delivery of neddylated proteins to proteasome could be compromised in HD. Under such circumstances, delivery of poly-neddylated huntingtin aggregates to autophagosome is more desirable and function of HYPK remains important.

DISCUSSION

The term proteostasis defines a conglomerate of processes that regulate the quality and quantity of cellular proteome. The proteostatic processes perform the critical functions in folding, oligomerization, post-translational modifications and degradation of proteins. While proteasomal degradation of abnormally folded and non-functional proteins is a global process, autophagy is more regulated, and it is tailored to clear the more specialized substrates like protein aggregates. Aggrephagy is specific form of autophagy that degrades the protein aggregates. The mechanism of aggrephagy exploits the delivery of lysine-63 linked poly-ubiquitinated protein aggregates to autophagosome by the help of different autophagic proteins. Given the complexity of the autophagy process, it is reasonable to contemplate that autophagy can be initiated by the intriguing activity of different regulatory proteins and mechanisms. We have characterized HYPK as an autophagy inducing protein. HYPK acts as a scaffolding protein that binds to the Nedd8 of poly-neddylated proteins and LC3 during its modulatory function in aggrephagy.

HYPK binds to the Nedd8 by its C-terminal UBA domain. UBA domains are known to bind the ubiquitin or ubiquitin-like proteins that regulate protein degradation, DNA repair, transcription etc. (**34**). Owing to the unique distribution of amino acids in its sequence, HYPK-UBA has very less sequence similarity with other UBA domains of human proteins, except the second UBA domain of NUB1 protein. The HYPK-UBA is composed of charge-rich region and hydrophobic patches. The conserved charged (D94, E101) and hydrophobic (L113, G118) residues of HYPK-UBA help this domain to strongly bind to the Nedd8. Though these residues are necessary, they are not sufficient for mediating the binding of HYPK-UBA to Nedd8. The neighboring residues are hypothesized to facilitate this binding. The UBA domain is conserved in HYPK protein of all species, signifying that Nedd8 binding is an essential function of HYPK.

Binding to LC3 is the other major function of HYPK. This function is attributed to the N-terminal Y-type LIR of HYPK. The functionality of different LIRs depends upon the presence of aromatic amino acids in the LIRs (**35**). Y49 of HYPK is necessary for HYPK interaction with LC3. Deletion of this conserved tyrosine residue abolishes the LC3 binding function of HYPK. The LIR is in the disordered N-terminal region of HYPK which imparts flexibility to LIR in terms of reaching the LC3 and bringing it close to the HYPK protein, thereby favoring the formation of autophagosome.

HYPK is a novel autophagic protein. It delivers the poly-neddylated protein aggregates to autophagosome (**Figure 9**). HYPK functions as a scaffolding protein which simultaneously tethers the Nedd8 and LC3. The aggregation-prone huntingtin exon1, in its poly-neddylated form, is a substrate of

HYPK dependent aggrephagy. Nevertheless, we speculate that the role of HYPK in poly-neddylation dependent autophagy is a general function of the protein. The annular-shaped structures of HYPK, i.e. H-granules, play important part in the aggrephagy process. The seeded amyloid-like nucleation of HYPK around the poly-neddylated huntingtin exon1 forms the H-granules that ensure rapid accumulation of HYPK around the Htt97Qexon1 aggregates. This leads to increased deposition of LC3 surrounding the poly-neddylated aggregates. In this respect, HYPK function is like p62 (SQSTM1) protein, except the fact that p62 is the scaffolding protein for poly-ubiquitinated protein aggregates (**36**) and HYPK has similar function for poly-neddylated proteins. Because HYPK and p62 are aggregation-prone proteins (**20, 37**), they probably induce autophagy by the similar mechanism.

We expect the functional importance of HYPK in Huntington's disease and in other neurodegenerative disorders. Since HYPK expression is less-to-moderate in different neurodegenerative disorders, there is a good scope of brain-specific upregulation of HYPK expression by small molecule modulators to mitigate the challenges of neuronal protein aggregates.

Redundancy of the post-translational modifications in protein degradation pathways are part of the fail-safe mechanism. While poly-ubiquitinated proteins can be degraded by proteasomal and autophagy pathways (**38**), previous report suggests that the poly-neddylated proteins can also be degraded by proteasome (**39**). In this study, we show that the poly-neddylated proteins, like poly-neddylated huntingtin exon1, can also be cleared by autophagy pathway. Thus, Nedd8 can functionally complement ubiquitin in both the proteasomal and autophagy pathways. Though the poly-ubiquitination and poly-neddylation dependent autophagy coexists, evolution of different kinds of neddylation and ubiquitination linkages may pose additional specificity and sensitivity towards neddylated autophagosed substrates. Contrary to the huge number of proteins that are poly-ubiquitinated, the number of proteins undergoing poly-neddylation is limited. Additionally, Nedd8 conjugation to the substrate proteins by culin-ligases may have more regulations in the autophagy.

Nedd8 has modulatory roles in neurodegenerative diseases. Nedd8 is accumulated in inclusion bodies (**40**). Moreover, the expression of Nedd8 and NUB1 are repressed in HD. This can downgrade the neddylation of proteins and their delivery to proteasome. In such condition, accelerated delivery of neddylated protein aggregates to autophagy vacuoles becomes as a viable prospect.

ACKNOWLEDGEMENTS

The authors extend their thankfulness to the DBT-IPLS of University of Calcutta (India), Indian Institute of Science Education and Research-Kolkata (IISER-Kolkata, India) and the Biocluster of National Centre for Biological Sciences (NCBS, India) for providing the ITC, SEM and TEM facilities respectively. The authors also thank the laboratory members of CFG for giving critical inputs in different experiments and reading the manuscript. The workforce of the sophisticated equipment facility of the research support service group of CDFD is acknowledged for their helps in different instrument operations. The research in the CFG group is generously supported by the core grants of CDFD. DKG and AJR were recipients of the graduate study fellowships from the council for scientific and industrial research (CSIR, Government of India).

AUTHOR CONTRIBUTIONS

The hypothesis and experimental schemes of the study were jointly conceived by AKR and DKG. DKG performed all experiments. AJR had contributed in the cloning, ITC and confocal microscopy experiments. AKR mentored the study, along with performing the tasks of data analysis and fund arrangements. AKR and DKG together wrote the paper.

CONFLICT OF INTEREST

The authors have no competing conflict of interest to disclose.

METHODS

Cloning

To clone the open reading frames (ORFs) of different genes, total RNA was isolated from IMR-32 cells (human neuroblastoma), and cDNAs of corresponding mRNAs were made by reverse transcription using the oligo-dT primer. ORFs of genes were amplified from cDNAs by polymerase chain reaction (PCR) using specific primer sets. The following clones were generated in specific vectors (see the results for the details of clones):

HYPK was cloned in pET21b, mCherry-pcDNA3.1(+), pEGFP-N1, pcDNA3.1(+) (C-terminal FLAG tagged).
HYPK-UBA (the UBA domain of HYPK) was cloned in pET21b, mCherry-pcDNA3.1(+), pcDNA3.1(+) (C-terminal FLAG tagged).
HYPK-UBA D94A, E101A (HYPK's UBA domain in which the D94 and E101 residues were mutated to alanine) and HYPK-UBA ΔL113, ΔG118 (HYPK's UBA domain that had deletions of L113 and G118) were cloned in pET21b.
HYPK-N60 (N-terminal 60 amino acid region of HYPK) and HYPK-Δ^{48}DYA^{50} (HYPK mutant in which the D48, Y49 and A50 residues were deleted) were cloned in pET21b and pEGFP-N1.
HYPK-C69 (C-terminal 69 residue region of HYPK) was cloned in pET21b, pEGFP-N1 and pcDNA3.1(+) (C-terminal FLAG tagged).
HYPK-N84 (N-terminal 84 amino acid region of HYPK) was cloned in mCherry-pcDNA3.1(+), pcDNA3.1(+).
Nedd8 was cloned pET21b, pcDNA3.1(+) and pSBFP2-C1.
LC3 was cloned in mCherry-pcDNA3.1(+) and pET21b.
ATG-5 was cloned in mOrange2-N1.
ATG-12 was cloned in mCherry-pcDNA3.1(+).
Htt97Qexon1 was cloned in pET21b, pEGFP-N1, pcDNA3.1(+).
Htt97Qexon1-GFP was cloned in pcDNA3.1(+).
HYPK along with either of LC3, GABARAP, GABARAPL1 and GABARAPL2 were cloned in pETDuet-1 vector. Similarly, LC3 along with either of HYPK, HYPK-N60, HYPK-C69 and HYPK-Δ^{48}DYA^{50} was cloned in pETDuet-1.

Deletion mutants of HYPK were made by using specific primer sets in the normal or overlapping PCR-based methods. FLAG peptide sequence was introduced to different clones by incorporating the sequence in-frame in the C-terminus by using the reverse primer. Lysine-to-arginine mutant of Nedd8 was constructed by specific primer sets using nested PCR methods. 6xHistidine was introduced to this mutant clone by incorporating its corresponding nucleotide sequence in-frame in the 5' region of forward primer

shRNAs of HYPK, ATG-5, Nedd8 and control (GFP) were cloned in pSUPER plasmid.

Details of clone maps, sequences of primers set(s) and shRNAs are available on request. The overall cloning process was similar to what was described in our previous studies (**20, 41**). Restriction digested PCR products and plasmids were ligated, followed by the transformation of the ligated

products into ultra-competent DH5α strain of *Escherichia coli*. Positive clones were selected by colony PCR. All clones were sequenced at the sophisticated equipment facility of the research support service group of CDFD.

Recombinant protein production and purification

The HYPK, HYPK-UBA, HYPK-UBA D94A, E101A, HYPK-UBA ΔL113, ΔG118, HYPK-N60, HYPK-C69, HYPK-Δ^{48}DYA^{50}, LC3, Nedd8, Htt97Qexon1 recombinant proteins were produced from pET21b vectors by the T7 approach that was described by us in earlier studies (**20, 42**). In the pETDuet-1 vector system, HYPK/ HYPK-N60/ HYPK-C69/ HYPK-Δ^{48}DYA^{50} and LC3A/ LC3B/ GABARAP/ GABARAPL1/ GABARAPL2 were 6xHis tagged and the interacting proteins (LC3 and HYPK) were untagged. The bacterial expressible clones were separately transformed into the BL21DE3 strain of *Escherichia coli*, followed by induction of protein synthesis by the application of IPTG (1mM final concentration) in the medium (LB-ampicillin). After 12-18 hours of protein production at 18°C, bacterial cells were lysed by sonication in the lysis buffer [50mM Tris-Cl (pH: 8.0), 300mM NaCl, 10mM imidazole, 1mM PMSF]. The cell lysate was cleared by centrifugation, followed by purification of the proteins in the nickel ion-based affinity exchange column chromatography. The cleared lysate was run through the Ni-NTA beads of column to allow the binding of the 6xHistidine (of the recombinant proteins) to the beads. The beads were subsequently washed with the wash buffer [50mM Tris-Cl (pH: 8.0), 300mM NaCl, 40mM imidazole], followed by elution of the proteins in elution buffer [50mM Tris-Cl (pH: 8.0), 300mM NaCl, 300mM imidazole]. Different proteins were dialyzed in different dialysis buffers depending upon the requirements of downstream assays. In all assays, >98% pure proteins were used.

Surface plasmon resonance

The properties of Nedd8 binding with HYPK, HYPK-UBA, HYPK-UBA D94A, E101A and HYPK-UBA ΔL113, ΔG118 were done by surface plasmon resonance (SPR) studies. Using the NHS/ EDC reagent, 5nmole of Nedd8 [in acetate buffer (pH: 4.0)] was immobilized on CM5 sensor chip by amine coupling. The mobile phase analytes (HYPK, HYPK-UBA, HYPK-UBA D94A, E101A and HYPK-UBA ΔL113, ΔG118) were kept in HBS-EP buffer [10mM HEPES (pH: 7.5), 150mM NaCl, 3mM EDTA, 0.005% (v/v) Surfactant P20 (pH: 7.4)]. Analyte to ligand binding experiments were done in the Biacore 3000 instrument at 25°C. Analytes were injected at a flowrate of 30µl/min, and the dissociation events lasted for 10 minutes. Concentrations of analytes were in the range of 40nM-25µM. Subtraction of the nonspecific binding from the actual binding response was done by measuring the binding in the mock immobilized surface of another channel. Dissociation constant [K_d] was measured by following 1:1 Langmuir model of dissociation.

Isothermal titration calorimetry

Isothermal titration calorimetry (ITC) experiments were conducted to measure the binding of LC3 protein with HYPK, HYPK-N60, HYPK-C69 and HYPK-Δ^{48}DYA^{50}. The protein-protein interaction studies were done in the MicroCal iTC 200 isothermal titration calorimeter instrument. The procedure of ITC was similar to our previous studies (**43, 44**). All proteins were kept in PBS (pH: 7.4) buffer. A thermostat maintained the temperature at 25°C for all the experiments. The cell proteins' (HYPK, HYPK-N60, HYPK-

C69, HYPK-Δ^{48}DYA^{50}) concentrations were 20µM and the syringe protein (LC3) concentration was 200µM.

The ITC instrument was run with the following parameters: a total 20 binding events were performed, the reference power of instrument was kept at 10 µcal/sec., time spacing of the binding events were 120 seconds and the syringe rotation speed was 300rpm.

Scanning electron microscopy

Individual proteins [HYPK, Htt97Qexon1, neddylated Htt97Qexon1 (Nedd8 cross-linking to Htt97Qexon1 was done by DSS cross-linking method)] or different protein complexes (Htt97Qexon1+HYPK, Neddylated Htt97Qexon1+HYPK, neddylated Htt97Qexon1+HYPK+LC3) were kept in 20mM Tris-Cl (pH: 8.0) buffer (in ultrapure water). A droplet of protein solution was casted on a cleaned glass coverslip, followed by air-drying of the droplet in the dust-free chamber. Air-dried proteins were washed with ultrapure water, and they were sequentially dried by air and gentle stream of nitrogen gas. Proteins were coated with a thin layer of gold-palladium mixture. Image acquisition was done in SUPRA 55VP field emission scanning electron microscope. The resolutions of the images were adjusted by keeping variable aperture diameter and electron beam voltage (80-100 kV) of the microscope.

Cell culture

Mouse neuroblastoma (Neuro2a) and human neuroblastoma (IMR-32) cells were procured from the National Centre for Cell Sciences (NCCS, India). Cells were cultured in AMEM medium which was supplemented with 10% fetal bovine serum, 2mM L-glutamine and 1x antibiotic-antimycotic solution. Cells were maintained at 37°C with 5% CO_2 in a humified incubator. Clones/ plasmids were transfected into the cells using Lipofectamine 2000 (Thermo Fischer Scientific) and Opti-MEM medium following manufacturer's instructions. shRNAs were transfected into cells using Lipofectamine 3000 (Thermo Fischer Scientific). The transfected cells were harvested 36 hours post-transfection. In the time-chase experiments, cells were intermittently harvested at every 12 hours up to 36 hours post-transfection. The final concentrations of MG132 (Sigma Aldrich, Cat. No. M8699), Chloroquine (Sigma Aldrich, Cat. No. C6628), MLN4924 (Sigma Aldrich, Cat. No. 5.05477) and MLN7243 (Takeda Pharmaceuticals Inc.) were 20µM in the cell culture medium. Cells were incubated with these chemicals for 0-36 hours depending upon the experimental requirements (see results).

Immunoprecipitation and Immunoblotting

Immunoprecipitation (IP) experiments of different cellular proteins were done by crosslink magnetic IP/co-IP method (Pierce Crosslink Magnetic IP/co-IP kit, Thermo Fischer Scientific, Cat. No. 88805) following the manufacturer's protocol. Some IP experiments were conducted in denaturing conditions (with 1% SDS). Following antibodies were used to immunoprecipitate different proteins: Nedd8 antibody v-15 (goat polyclonal, Santa Cruz Biotechnology, Cat. No: sc5480) and anti-HYPK antibody (Sigma Aldrich, Cat. No: HPA055252) and anti-polyHistidine antibody (Sigma Aldrich, Cat. No: H1029).

In the immunoblotting experiments, cells were harvested and lysed in pre-chilled lysis buffer [150mM NaCl, 1% NP-40, 0.5% sodium deoxycholate, 0.1% SDS, 50mM Tris-Cl (pH: 8.0), and protease inhibitor cocktail]. Lysis was completed by keeping the cell suspension in lysis buffer at 4°C for 2 hours. Total cellular protein was acetone-precipitated, followed by re-solubilization of the proteins in the solubilization buffer [50mM Tris-Cl (pH – 8.0), 50mM NaCl]. Protein concentrations were estimated by standard Bradford assays. 40-60µg of protein was separated in 12% SDS-PAGE, followed by the immunoblotting steps that involved the transfer of proteins to PVDF membrane and sequential use of primary and secondary antibodies. Intermittent washing steps were done by TBST buffer (pH: 7.4). The following primary antibodies were used: anti-HYPK antibody (Sigma Aldrich, HPA055252; dilution - 1:2000), anti-LC3 antibody - APG8A (Sigma Aldrich, SAB 1305639; dilution – 1:2000), anti-Nedd8 antibody v-15 (Santa Cruz Biotechnology, sc5480; dilution – 1: 2500) [the anti-Nedd8 antibody was raised against an N-terminal peptide of human Nedd8. Since the sequence of this peptide region was not similar to ubiquitin, the anti-Nedd8 antibody was not detected to recognize the ubiquitin protein], anti-polyglutamine antibody - 3B5H10 (Sigma Aldrich, P1874; dilution – 1:2500), anti-Beclin-1 antibody (Abcam, ab62557; dilution – 1:3500), anti-ATG-5 antibody (Sigma Aldrich, A0856; dilution – 1:2000), anti-FLAG antibody (Sigma Aldrich, F3165; dilution – 1:5000), anti-GFP antibody (Sigma Aldrich, SAB2702197; dilution – 1:2500), anti-polyHistidine antibody (Sigma Aldrich, Cat. No: H1029), anti-beta tubulin antibody – AA2 (Sigma Aldrich, T8328; dilution – 1:5000). The following secondary antibodies were used: anti-goat IgG (whole molecule) peroxidase antibody produced in rabbit (Sigma Aldrich, A8919; dilution – 1:5000), anti-rabbit IgG (whole molecule) peroxidase antibody produced in goat (Sigma Aldrich, A0545; dilution – 1:5000), anti-mouse IgG (whole molecule) peroxidase antibody produced in rabbit (Sigma Aldrich, A9044; dilution – 1:5000).

Fluorescence microscopy

Adherent IMR-32 or Neuro2a cells were washed with PBS (pH: 7.4), followed by crosslinking with paraformaldehyde (4%, in PBS). EGFP, mCherry, mOrange2 and BFP expressing cells were directly imaged for fluorescence signals. In immunocytochemistry, cells were treated with 0.2% TritonX-100 (in PBS, pH: 7.4) for permeabilization, followed by blocking with 1% BSA (in PBS, pH: 7.4). The next steps involved the sequential application of primary and secondary antibodies. The following primary antibodies were used: anti-HYPK antibody (Sigma Aldrich, HPA055252; dilution - 1:350), anti-LC3 antibody - APG8A (Sigma Aldrich, SAB 1305639; dilution – 1:400) and anti-Beclin-1 antibody (Abcam, ab62557; dilution – 1:350). The following secondary antibodies were used: goat anti-rabbit IgG (H+L) secondary antibody-Alexa fluor 488 (Thermo Fischer Scientific A,-11008; dilution – 1:400), goat anti-rabbit IgG (H+L) secondary antibody-Alexa fluor 647 (Thermo Fischer Scientific, A -21245; dilution – 1:400), goat anti-mouse IgG (H+L) secondary antibody-Alexa fluor 647 (Thermo Fischer Scientific, A -21235; dilution – 1:400), goat anti-rabbit IgG (H+L) superclonal secondary antibody-Alexa fluor 555 (Thermo Fischer Scientific, A -27039; dilution – 1:400), anti-rabbit IgG whole molecule-TRITC produced in goat (Sigma Aldrich, 6778; dilution – 1:400). Cells were mounted in DAPI-containing mounting medium (Fluoroshield).

Image acquisition was done in Zeiss LSM700 meta-confocal microscope (Carl Zeiss Microimaging Inc.) with the 63x Plan-Apo/ 1.4 NA oil/ DIC objectives. All images were processed in Zen-Lite (black) software (Carl Zeiss Microimaging Inc.).

Colocalization analysis of different proteins were done in Zen-Lite (Blue edition) software (Carl Zeiss Microimaging Inc.) by using the colocalization algorithm. The Pearson's correlation coefficient was used as a measure of colocalization of proteins.

Counting of LC3 puncta and neurite-forming cells in different conditions were done by live-cell imaging in Nikon live-cell imaging system/stereomicroscope.

Transmission electron microscopy

IMR-32 cells were grown in culture dishes. HYPK or Htt97Qexon1 + HYPK were transfected into cells by the procedure that was mentioned in the cell culture section. Detached cells were fixed in 1.5% (v/v) glutaraldehyde/ 4% (w/v) formaldehyde (in 0.1M cacodylate buffer, pH - 7.3) solution for five hours, followed by washing of the cells with PBS (pH: 7.4) for few times. Gradual dehydration of the cells was done by sequentially keeping them in 50%, 70% and 90% ethanol (15 minutes/ solution). Cells were sectioned (1µm thick) in ultra-microtome before placing them on copper grid (200 mesh). Section containing grids were incubated in 0.05M glycine (in PBS, pH: 7.4) for 20 minutes. Grids were then washed with PBS (pH: 7.4), followed by staining with aqueous uranyl acetate for 2 minutes. After the grids were washed with water, they were transiently (for 15 seconds) exposed to lead citrate. Images were collected in Tecnai G2 Spirit Bio-TWIN transmission electron microscope. Electron beam strength was 15kV and images were recorded in Gatan Orins CCD camera.

Fluorescence activated cell sorting

Fluorescence activated cell sorting was done to analyze the number of apoptotic cells and the pattern of cell cycle stages during differential expression of Htt97Qexon1 and HYPK in IMR-32 cells. Cells were detached from dishes by trypsin-EDTA treatment, followed by washing of the cells with PBS (pH: 7.4) for few times. Cells were resuspended and incubated in 500µl PBS (pH: 7.4) which contained 20µl of 0.1% TritonX-100, 50µl of 100mg/ml Ribonuclease-A and 300µl of 50µg/ml propidium iodide at room temperature for 15 minutes (constant mixing). Apoptotic cells were detected by using Annexin V-FITC apoptosis detection kit (Sigma Aldrich, Cat. No: APOAF) by following manufacturer's protocol. Briefly, trypsinized cells were washed with PBS and they were incubated with appropriate volumes of Annexin V-FITC and propidium iodide solutions, followed by incubation of cells at room temperature for 15 minutes in constant mixing mode. FACS experiments were done in the BD-FACSARIA-III (Becton Dickenson Biosciences) instrument. Analyses were conducted in the BD-FACSDIVA software.

Computational studies

Sequence alignment: The sequences of UBA domains of different human proteins were curated from the SMART database (**45**). The HYPK sequences of different organisms and sequences of LC3

interacting proteins were obtained from protein database of NCBI. The alignments of sequences were done in Clustal Omega (**46**).

Phylogenetic analysis: The sequence alignment file of the UBA domains was saved in the phylip (.phy) format which was analyzed in the Phylip-3.695 software package. The Seqboot, Protdist, Neighbor and Consense programs were sequentially run to analyze the phylogeny of the UBA domains of different human proteins. The outfile of each program was taken as the input file of the next program. Details of the parameters of each program are available upon request. The cladogram was generated in the Treeview software. The process of phylogenetic analysis followed the same set of steps as described in our previous study (**47**).

GEO profile analysis: Gene/ transcript expression profiles of Nedd8, NUB1, and NAE1 were curated from the datasets of Gene Expression Omnibus (GEO) repository of NCBI. The expression of the above genes was analyzed in Huntington's disease mice versus control mice by comparing the transcript quantity from the following GEO profiles: GDS4533, GDS4534, GDS2912. Expression level of HYPK were curated from GEO profiles of different neurodegenerative disorders, brain related diseases and stresses were taken from GEO database. Following GEO profiles were analyzed for evaluation – neurodegenerative and brain related diseases: GDS2821, GDS810, GDS3408, GDS3459, GDS3730, GDS4414, GDS3545, GDS3544, GDS4218, GDS4553, GDS1917, GDS1912, GDS2914, GDS4214, GDS4012, GDS4467, GDS1331; Stress: GDS3365, GDS3383, GDS2054, GDS1317, GDS4104, GDS324, GDS1500, GDS1794, GDS246, GDS738, GDS4849, GDS3463, GDS3135.

HYPK interacting protein analysis: The HYPK interacting proteins were curated from the BIOGRID (**48**) and STRING (**49**) databases.

Aggregation-prone region analysis: Aggregation prone regions in HYPK interacting proteins were predicted in Waltz web server (http://www.switchlab.org/bioinformatics/waltz) and Aggrescan3D web server (http://biocomp.chem.uw.edu.pl/A3D/) (**50**). We had previously used this process to find the aggregation-prone regions of $SOD1^{G85R}$ and $SOD1^{G93A}$ (**51**).

Nedd8 structure: The Nedd8 structure was obtained from the protein data bank (PDB code: 1NDD) (**52**).

Statistical analysis

The comparisons of means among groups were done by t-test.

Graphics

The graphics of constructs were generated in Adobe Illustrator. The graphs were generated in the Graphpad Prism software.

REFERENCES

1. Labbadia, J., and R.I. Morimoto. 2015. The biology of proteostasis in aging and disease. *Annu Rev Biochem*. 84:435-464.
2. Klaips, C.L., G.G. Jayaraj, and F.U. Hartl. 2018. Pathways of cellular proteostasis in aging and disease. *J Cell Biol*. 217:51-63.
3. Hartl, F.U., A. Bracher, and M. Hayer-Hartl. 2011. Molecular chaperones in protein folding and proteostasis. *Nature*. 475:324-332.
4. Chakrabarti, A., A.W. Chen, and J.D. Varner. 2011. A review of the mammalian unfolded protein response. *Biotechnol Bioeng*. 108:2777-2793.
5. Karve, T.M., and A.K. Cheema. 2011. Small changes huge impact: the role of protein posttranslational modifications in cellular homeostasis and disease. *J Amino Acids*. 2011:207691.
6. Varshavsky, A. 2005. Regulated protein degradation. *Trends Biochem Sci*. 30:283-286.
7. Ciechanover, A., and Y.T. Kwon. 2015. Degradation of misfolded proteins in neurodegenerative diseases: therapeutic targets and strategies. *Exp Mol Med*. 47:e147.
8. Swatek, K.N., and D. Komander. 2016. Ubiquitin modifications. *Cell Res*. 26:399-422.
9. Glick, D., S. Barth, and K.F. Macleod. 2010. Autophagy: cellular and molecular mechanisms. *J Pathol*. 221:3-12.
10. Lamark, T., and T. Johansen. 2012. Aggrephagy: selective disposal of protein aggregates by macroautophagy. *Int J Cell Biol*. 2012:736905.
11. Yamamoto, A., and A. Simonsen. 2011. The elimination of accumulated and aggregated proteins: a role for aggrephagy in neurodegeneration. *Neurobiol Dis*. 43:17-28.
12. Hyttinen, J.M., M. Amadio, J. Viiri, A. Pascale, A. Salminen, and K. Kaarniranta. 2014. Clearance of misfolded and aggregated proteins by aggrephagy and implications for aggregation diseases. *Ageing Res Rev*. 18:16-28.
13. Wani, W.Y., M. Boyer-Guittaut, M. Dodson, J. Chatham, V. Darley-Usmar, and J. Zhang. 2015. Regulation of autophagy by protein post-translational modification. *Lab Invest*. 95:14-25.
14. Fan, M., R.M. Bigsby, and K.P. Nephew. 2003. The NEDD8 pathway is required for proteasome-mediated degradation of human estrogen receptor (ER)-alpha and essential for the antiproliferative activity of ICI 182,780 in ERalpha-positive breast cancer cells. *Mol Endocrinol*. 17:356-365.
15. Soucy, T.A., L.R. Dick, P.G. Smith, M.A. Milhollen, and J.E. Brownell. 2010. The NEDD8 Conjugation Pathway and Its Relevance in Cancer Biology and Therapy. *Genes Cancer*. 1:708-716.
16. Walden, H., M.S. Podgorski, D.T. Huang, D.W. Miller, R.J. Howard, D.L. Minor, Jr., J.M. Holton, and B.A. Schulman. 2003. The structure of the APPBP1-UBA3-NEDD8-ATP complex reveals the basis for selective ubiquitin-like protein activation by an E1. *Mol Cell*. 12:1427-1437.
17. Xirodimas, D.P. 2008. Novel substrates and functions for the ubiquitin-like molecule NEDD8. *Biochem Soc Trans*. 36:802-806.
18. Zhou, L., W. Zhang, Y. Sun, and L. Jia. 2018. Protein neddylation and its alterations in human cancers for targeted therapy. *Cell Signal*. 44:92-102.
19. Chen, Y., R.L. Neve, and H. Liu. 2012. Neddylation dysfunction in Alzheimer's disease. *J Cell Mol Med*. 16:2583-2591.
20. Ghosh, D.K., A. Roy, and A. Ranjan. 2018. Aggregation-prone Regions in HYPK Help It to Form Sequestration Complex for Toxic Protein Aggregates. *J Mol Biol*. 430:963-986.
21. Ghosh, D.K., A. Roy, and A. Ranjan. 2018. Disordered Nanostructure in Huntingtin Interacting Protein K Acts as a Stabilizing Switch To Prevent Protein Aggregation. *Biochemistry*. 57:2009-2023.

22. Raychaudhuri, S., M. Sinha, D. Mukhopadhyay, and N.P. Bhattacharyya. 2008. HYPK, a Huntingtin interacting protein, reduces aggregates and apoptosis induced by N-terminal Huntingtin with 40 glutamines in Neuro2a cells and exhibits chaperone-like activity. *Hum Mol Genet*. 17:240-255.
23. Arnesen, T., K.K. Starheim, P. Van Damme, R. Evjenth, H. Dinh, M.J. Betts, A. Ryningen, J. Vandekerckhove, K. Gevaert, and D. Anderson. 2010. The chaperone-like protein HYPK acts together with NatA in cotranslational N-terminal acetylation and prevention of Huntingtin aggregation. *Mol Cell Biol*. 30:1898-1909.
24. Choudhury, K.R., S. Raychaudhuri, and N.P. Bhattacharyya. 2012. Identification of HYPK-interacting proteins reveals involvement of HYPK in regulating cell growth, cell cycle, unfolded protein response and cell death. *PLoS One*. 7:e51415.
25. Ayyadevara, S., M. Balasubramaniam, Y. Gao, L.R. Yu, R. Alla, and R. Shmookler Reis. 2015. Proteins in aggregates functionally impact multiple neurodegenerative disease models by forming proteasome-blocking complexes. *Aging Cell*. 14:35-48.
26. Bell, R., A. Hubbard, R. Chettier, D. Chen, J.P. Miller, P. Kapahi, M. Tarnopolsky, S. Sahasrabuhde, S. Melov, and R.E. Hughes. 2009. A human protein interaction network shows conservation of aging processes between human and invertebrate species. *PLoS Genet*. 5:e1000414.
27. Lu, B., I. Al-Ramahi, A. Valencia, Q. Wang, F. Berenshteyn, H. Yang, T. Gallego-Flores, S. Ichcho, A. Lacoste, M. Hild, M. Difiglia, J. Botas, and J. Palacino. 2013. Identification of NUB1 as a suppressor of mutant Huntington toxicity via enhanced protein clearance. *Nat Neurosci*. 16:562-570.
28. Liu, S., H. Yang, J. Zhao, Y.H. Zhang, A.X. Song, and H.Y. Hu. 2013. NEDD8 ultimate buster-1 long (NUB1L) protein promotes transfer of NEDD8 to proteasome for degradation through the P97UFD1/NPL4 complex. *J Biol Chem*. 288:31339-31349.
29. Macharia, M.W., W.Y.Z. Tan, P.P. Das, N.I. Naqvi, and S.M. Wong. 2019. Proximity-dependent biotinylation screening identifies NbHYPK as a novel interacting partner of ATG8 in plants. *BMC Plant Biol*. 19:326.
30. Ye, C., Y. Zhang, W. Wang, J. Wang, and H. Li. 2008. Inhibition of neurite outgrowth and promotion of cell death by cytoplasmic soluble mutant huntingtin stably transfected in mouse neuroblastoma cells. *Neurosci Lett*. 442:63-68.
31. Jacobsen, J.C., G.C. Gregory, J.M. Woda, M.N. Thompson, K.R. Coser, V. Murthy, I.S. Kohane, J.F. Gusella, I.S. Seong, M.E. MacDonald, T. Shioda, and J.M. Lee. 2011. HD CAG-correlated gene expression changes support a simple dominant gain of function. *Hum Mol Genet*. 20:2846-2860.
32. Lee, J.M., J. Zhang, A.I. Su, J.R. Walker, T. Wiltshire, K. Kang, E. Dragileva, T. Gillis, E.T. Lopez, M.J. Boily, M. Cyr, I. Kohane, J.F. Gusella, M.E. MacDonald, and V.C. Wheeler. 2010. A novel approach to investigate tissue-specific trinucleotide repeat instability. *BMC Syst Biol*. 4:29.
33. Hodges, A., G. Hughes, S. Brooks, L. Elliston, P. Holmans, S.B. Dunnett, and L. Jones. 2008. Brain gene expression correlates with changes in behavior in the R6/1 mouse model of Huntington's disease. *Genes Brain Behav*. 7:288-299.
34. Hochstrasser, M. 2009. Origin and function of ubiquitin-like proteins. *Nature*. 458:422-429.
35. Birgisdottir, A.B., T. Lamark, and T. Johansen. 2013. The LIR motif - crucial for selective autophagy. *J Cell Sci*. 126:3237-3247.
36. Moscat, J., and M.T. Diaz-Meco. 2009. p62 at the crossroads of autophagy, apoptosis, and cancer. *Cell*. 137:1001-1004.
37. Bjorkoy, G., T. Lamark, A. Brech, H. Outzen, M. Perander, A. Overvatn, H. Stenmark, and T. Johansen. 2005. p62/SQSTM1 forms protein aggregates degraded by autophagy and has a protective effect on huntingtin-induced cell death. *J Cell Biol*. 171:603-614.

38. Li, W., and Y. Ye. 2008. Polyubiquitin chains: functions, structures, and mechanisms. *Cell Mol Life Sci*. 65:2397-2406.
39. Enchev, R.I., B.A. Schulman, and M. Peter. 2015. Protein neddylation: beyond cullin-RING ligases. *Nat Rev Mol Cell Biol*. 16:30-44.
40. Mori, F., M. Nishie, Y.S. Piao, K. Kito, T. Kamitani, H. Takahashi, and K. Wakabayashi. 2005. Accumulation of NEDD8 in neuronal and glial inclusions of neurodegenerative disorders. *Neuropathol Appl Neurobiol*. 31:53-61.
41. Ghosh, D.K., A. Kumar, and A. Ranjan. 2018. Metastable states of HYPK-UBA domain's seeds drive the dynamics of its own aggregation. *Biochim Biophys Acta Gen Subj*. 1862:2846-2861.
42. Roy, A., R. Reddi, B. Sawhney, D.K. Ghosh, A. Addlagatta, and A. Ranjan. 2016. Expression, Functional Characterization and X-ray Analysis of HosA, A Member of MarR Family of Transcription Regulator from Uropathogenic Escherichia coli. *Protein J*. 35:269-282.
43. Kumar, A., D.K. Ghosh, J. Ali, and A. Ranjan. 2019. Characterization of Lipid Binding Properties of Plasmodium falciparum Acyl-Coenzyme A Binding Proteins and Their Competitive Inhibition by Mefloquine. *ACS Chem Biol*. 14:901-915.
44. Ghosh, D.K., and A. Ranjan. 2019. An IRES-dependent translation of HYPK mRNA generates a truncated isoform of the protein that lacks the nuclear localization and functional ability. *RNA Biol*:1-18.
45. Letunic, I., T. Doerks, and P. Bork. 2015. SMART: recent updates, new developments and status in 2015. *Nucleic Acids Res*. 43:D257-260.
46. Sievers, F., A. Wilm, D. Dineen, T.J. Gibson, K. Karplus, W. Li, R. Lopez, H. McWilliam, M. Remmert, J. Soding, J.D. Thompson, and D.G. Higgins. 2011. Fast, scalable generation of high-quality protein multiple sequence alignments using Clustal Omega. *Mol Syst Biol*. 7:539.
47. Ghosh, D.K., A. Roy, and A. Ranjan. 2018. The ATPase VCP/p97 functions as a disaggregase against toxic Huntingtin-exon1 aggregates. *FEBS Lett*. 592:2680-2692.
48. Stark, C., B.J. Breitkreutz, T. Reguly, L. Boucher, A. Breitkreutz, and M. Tyers. 2006. BioGRID: a general repository for interaction datasets. *Nucleic Acids Res*. 34:D535-539.
49. Szklarczyk, D., A. Franceschini, S. Wyder, K. Forslund, D. Heller, J. Huerta-Cepas, M. Simonovic, A. Roth, A. Santos, K.P. Tsafou, M. Kuhn, P. Bork, L.J. Jensen, and C. von Mering. 2015. STRING v10: protein-protein interaction networks, integrated over the tree of life. *Nucleic Acids Res*. 43:D447-452.
50. Zambrano, R., M. Jamroz, A. Szczasiuk, J. Pujols, S. Kmiecik, and S. Ventura. 2015. AGGRESCAN3D (A3D): server for prediction of aggregation properties of protein structures. *Nucleic Acids Res*. 43:W306-313.
51. Ghosh, D.K., A.N. Shrikondawar, and A. Ranjan. 2019. Local structural unfolding at the edge-strands of beta sheets is the molecular basis for instability and aggregation of G85R and G93A mutants of Superoxide dismutase 1. *J Biomol Struct Dyn*:1-17.
52. Whitby, F.G., G. Xia, C.M. Pickart, and C.P. Hill. 1998. Crystal structure of the human ubiquitin-like protein NEDD8 and interactions with ubiquitin pathway enzymes. *J Biol Chem*. 273:34983-34991.

FIGURES AND FIGURE LEGENDS

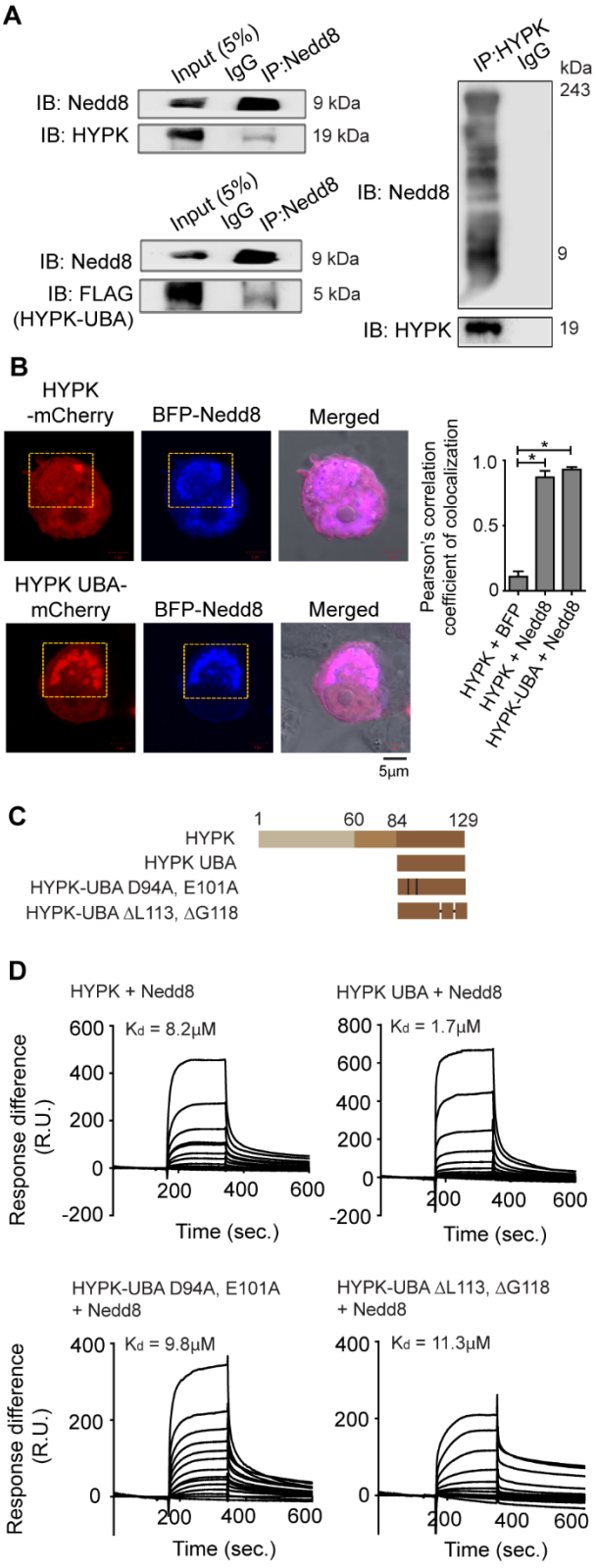

Figure 1. HYPK binds to the Nedd8 protein by its C-terminal UBA domain. (A) Immunoblotting of the immunecomplexes of endogenous Nedd8 [IP: Nedd8] and endogenous HYPK [IP: HYPK] from cell lysate of IMR-32 cells that were untransfected or transfected with HYPK-UBA [FLAG-tagged]. Immunoblotting was done with indicated antibodies. Immunoprecipitations were done in non-denaturing condition. (B) Representative confocal microscopy images of colocalization of HYPK-mCherry and HYPK-UBA-mCherry domain with the Nedd8-BFP protein in IMR-32 cells. [*HYPK-mCherry colocalization with Nedd8-BFP vs. BFP: $p < 0.001$, $n = 96$; *HYPK-UBA-mCherry colocalization with Nedd8-BFP vs. BFP: $p < 0.001$, $n = 89$]. (C) Schematic representation of HYPK, its UBA domain and different mutants of UBA domain. (D) Characterization of quantitative binding responses and affinities of interactions of recombinant HYPK, HYPK-UBA, HYPK-UBA D94A, E101A, HYPK-UBA ΔL113, ΔG118 with recombinant Nedd8 by SPR assays. Calculated dissociation constants [K_d value] are shown.

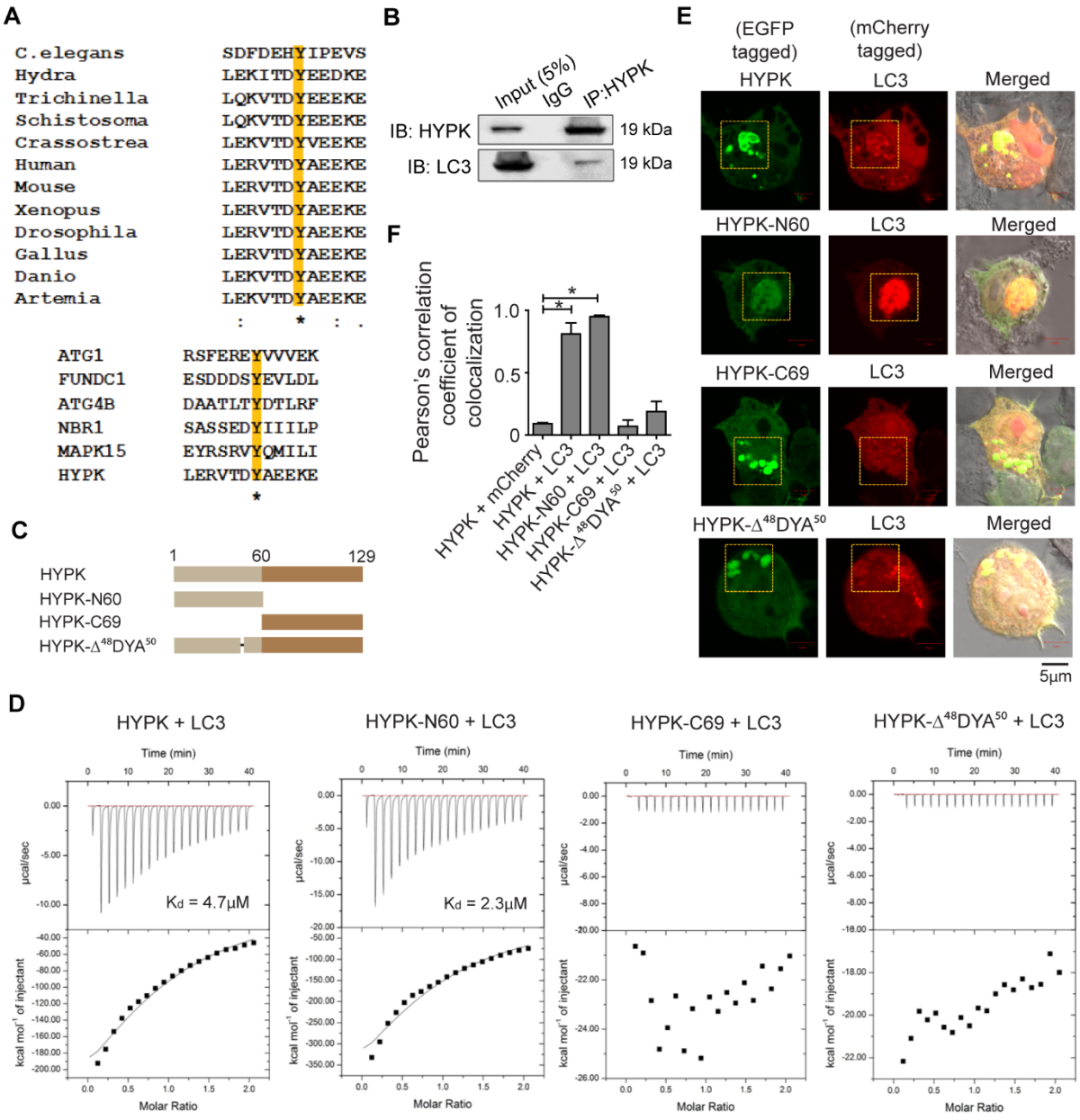

Figure 2. HYPK interacts with the LC3 proteins by its N-terminal LC3 interaction region. (A) [Upper panel] Alignment of the putative LIR sequences of HYPK proteins of different organisms. [Lower panel] Alignment of putative HYPK-LIR sequence with the sequences of tyrosine-type LIRs of other LC3 interacting proteins. (B) Immunoblotting of the immunecomplexes of endogenous LC3 [IP: LC3] from cell lysate of untransfected IMR-32 cells. Immunoblotting was done with indicated antibodies. The immunoprecipitation was done in non-denaturing condition. (C) Schematic representation of the HYPK and its different deletion mutant constructs. (D) ITC analysis of protein-protein interactions of recombinant HYPK, HYPK-N60, HYPK-C69 and HYPK-Δ^{48}DYA^{50} with recombinant LC3. Dissociation constant values [K_d] are indicated. (E) Representative confocal microscopy images of colocalization of HYPK-EGFP, HYPK-N60-EGFP, HYPK-C69-EGFP and HYPK-Δ^{48}DYA^{50}-EGFP with LC3-mCherry in IMR-32

cells. (F) Quantitative estimation of intracellular LC3 colocalization with HYPK, HYPK-N60, HYPK-C69 and HYPK-Δ^{48}DYA^{50} [*HYPK-EGFP colocalization with LC3-mCherry vs. mCherry: $p < 0.005$, $n = 117$; *HYPK-N60-EGFP colocalization with LC3-mCherry vs. mCherry: $p < 0.005$, $n = 71$].

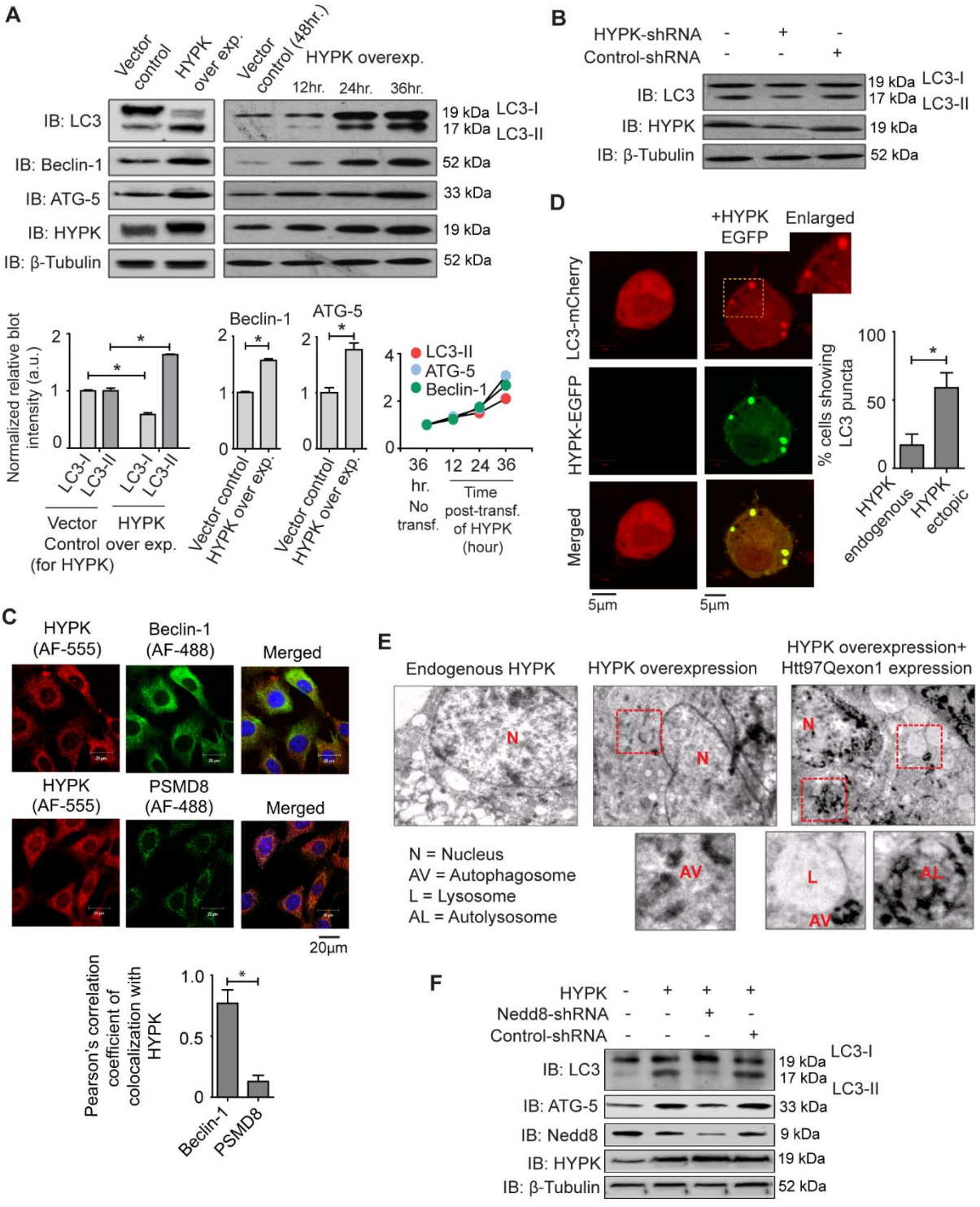

Figure 3. HYPK is an autophagy inducing protein. (A) [Upper left] Immunoblotting for LC3, beclin-1, ATG-5, HYPK and β-tubulin with indicated antibodies from lysate of IMR-32 cells that were transfected with vector [pcDNA3.1(+)] or HYPK. [Upper right] Immunoblots of LC3, beclin-1, ATG-5, HYPK and β-tubulin with indicated antibodies from HYPK transfected IMR-32 cell lysate in time-chase study. [Lower

902 panel] Densitometry of blots [*LC3-I and LC3-II expression in vector control vs. HYPK overexpression: $p <$
903 0.005, n = 3; *Beclin-1 expression in vector control vs. HYPK overexpression: $p < 0.005$, n = 3; *ATG-5
904 expression in vector control vs. HYPK overexpression: $p < 0.005$, n = 3]. (B) Immunoblots of LC3, HYPK
905 and β-tubulin with indicated antibodies from HYPK-shRNA or control [GFP]-shRNA transfected IMR-32
906 cell lysate. (C) Representative confocal microscopy image of HYPK colocalization with beclin-1, but not
907 with proteasomal protein PSMD8, in untransfected IMR-32 cells. [*HYPK colocalization with beclin-1 vs.
908 PSMD8: $p < 0.001$, n = 82]. (D) Confocal microscopy image of LC3-mCherry puncta formation in HYPK-
909 EGFP expressing IMR-32 cells. [*LC3 puncta formation in cells with endogenous HYPK expression vs.
910 HYPK-EGFP overexpression: $p < 0.005$, n = 65]. (E) Representative transmission electron microscopy
911 images of autophagy vacuoles and autolysosomes in IMR-32 cells that were untransfected or
912 transfected with HYPK and Htt97Qexon1. (F) Immunoblots of LC3, ATG-5, HYPK, Nedd8 and β-tubulin
913 with indicated antibodies from the lysates of IMR-32 cells that were untransfected or transfected with
914 HYPK, Nedd8-shRNA and control [GFP]-shRNA.
915
916
917
918
919
920
921
922
923
924
925
926
927
928
929
930
931
932
933
934
935
936
937
938
939
940
941
942
943

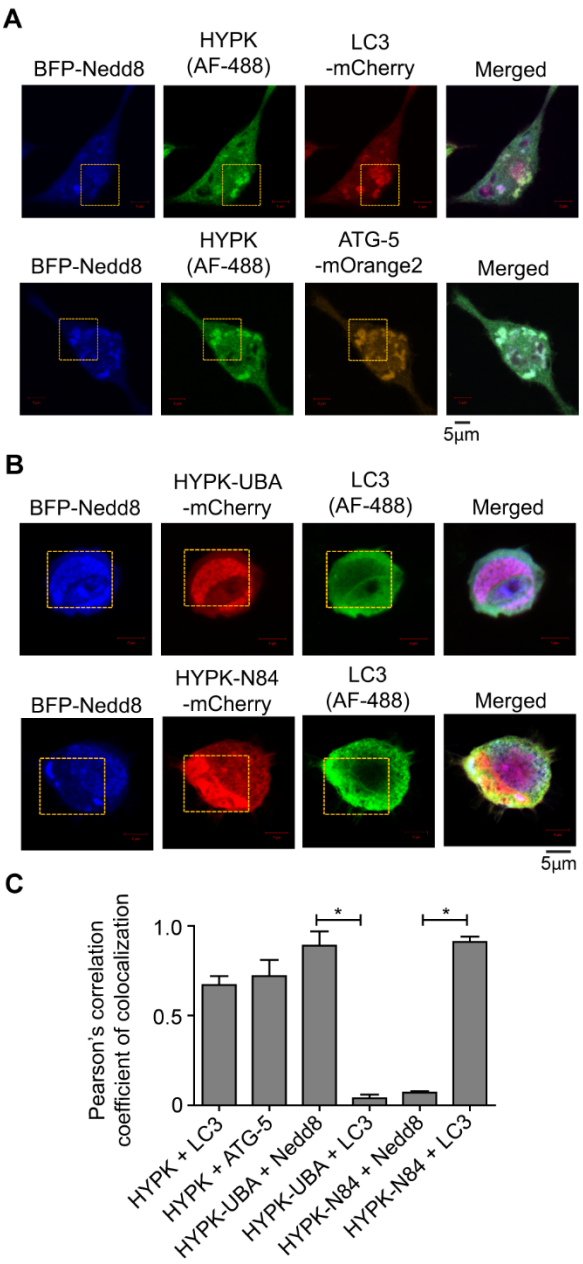

Figure 4. The individual domains of HYPK cannot simultaneously interact with the Nedd8 and LC3 proteins. (A) Representative confocal microscopy image of endogenous HYPK colocalization with BFP-Nedd8 and autophagy related proteins LC3-mCherry and ATG-5-mOrange2 in IMR-32 cells that were transfected with BFP-Nedd8, LC3-mCherry and ATG-5-mOrange2. (B) [Upper] Confocal microscopy image of HYPK-UBA-mCherry colocalization with BFP-Nedd8, but not with endogenous LC3, in IMR-32 cells that were transfected with BFP-Nedd8 and HYPK-UBA-mCherry. [Lower panel] Confocal microscopy image of HYPK-N84-mCherry colocalization with the endogenous LC3 protein, but not with BFP-Nedd8, in IMR-32 cells that were transfected with HYPK-N84-mCherry and BFP-Nedd8 [AF-488 is secondary antibody associated Alexa Fluor 488]. (C) Quantification of colocalization of HYPK, HYPK-UBA domain

and HYPK-N84 with LC3 and Nedd8 [*Colocalization of HYPK-UBA with Nedd8 vs. LC3: $p < 0.001$, $n = 70$; *colocalization of HYPK-N84 with Nedd8 vs. LC3: $p < 0.001$, $n = 75$].

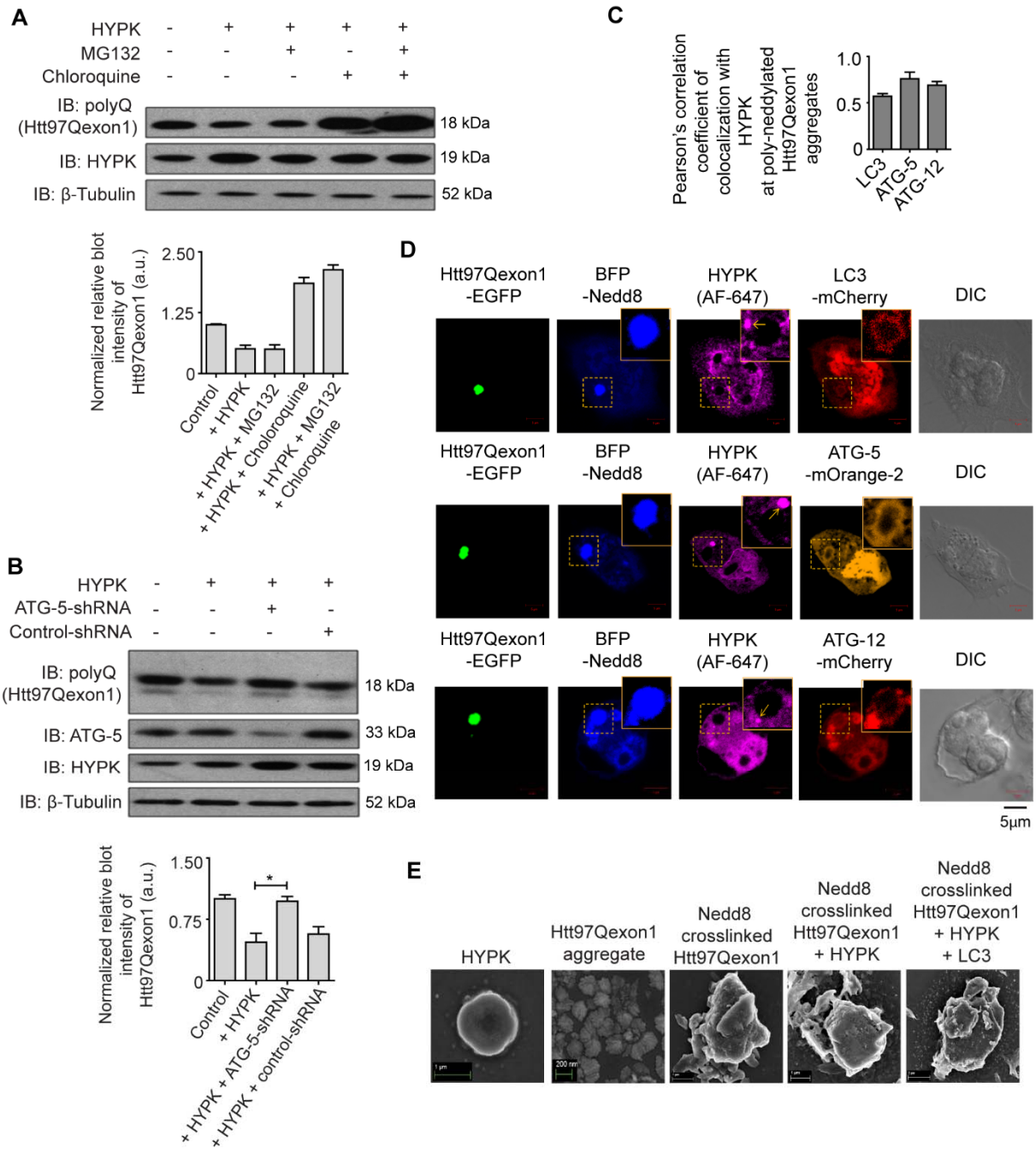

Figure 5. HYPK mediates autophagic clearance of the poly-neddylated huntingtin exon1 aggregates. The H-granules of HYPK helps in formation of the autophagosome around the poly-neddylated Htt97Qexon1 aggregates. (A) Immunoblotting for Htt97Qexon1, HYPK and β-tubulin with indicated antibodies from lysate of IMR-32 cells that were transfected with Htt97Qexon1, HYPK and treated with 20nM MG132 and/or 20nM chloroquine for 36 hours. [anti-polyQ antibody detects poly-glutamine expanded huntingtin, like Htt97Qexon1]. (B) Immunoblotting for Htt97Qexon1, ATG-5, HYPK and β-tubulin with indicated antibodies from lysate of IMR-32 cells that were transfected with Htt97Qexon1, HYPK, ATG-5-shRNA and control [GFP]-shRNA. [*Htt97Qexon1 level in HYPK vs. HYPK+ATG-5-shRNA: p <

0.005, n = 3]. (C) Quantification of colocalization of LC3, ATG-5 and ATG-12 with HYPK associated poly-neddylated Htt97Qexon1 in IMR-32 cells. (D) Representative confocal microscopy images of coassociation of endogenous HYPK and colocalization of BFP-Nedd8, LC3-mCherry, ATG-5-mOrange2, ATG-12-mCherry with Htt97Qexon1-GFP in the IMR-32 cells. Yellow arrows point the H-granules of HYPK [AF-647 is secondary antibody associated Alexa Fluor 647]. (E) Scanning electron micrographs of *In vitro* reconstituted complexes of different combinations of recombinant proteins of Htt97Qexon1, HYPK, LC3 and Nedd8 crosslinked Htt97Qexon1.

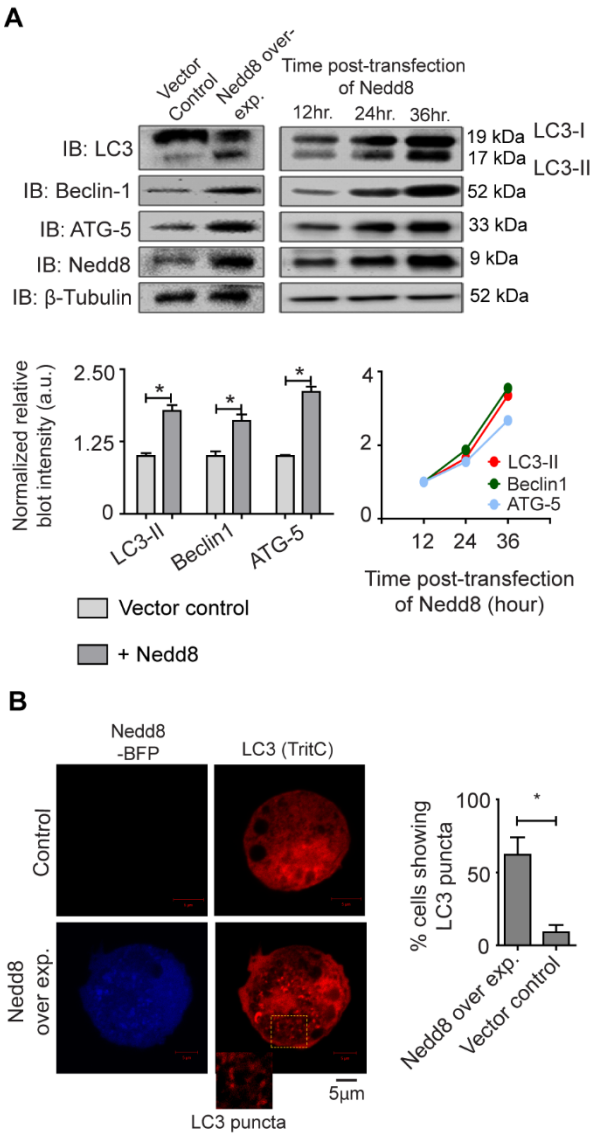

Figure 6. Nedd8 induces autophagy in IMR-32 cells. (A) [Upper left] Immunoblotting for LC3, beclin-1, ATG-5, Nedd8 and β-tubulin with indicated antibodies from lysate of IMR-32 cells that were untransfected or transfected with Nedd8. [Upper right] Immunoblotting for LC3, beclin-1, ATG-5, Nedd8 and β-tubulin with indicated antibodies in a time-chase assay from lysate of IMR-32 cells that were transfected with Nedd8. [Lower left] Densitometry of upper left blots [*LC3-II expression in vector control vs. Nedd8 overexpression: $p < 0.005$, $n = 3$; *beclin-1 expression in vector control vs. Nedd8 overexpression: $p < 0.005$, $n = 3$; *ATG-5 expression in vector control vs. Nedd8 overexpression: $p < 0.005$, $n = 3$]. [Lower right] Densitometry of upper right blots. (B) Representative confocal microscopy images of puncta formation of endogenous LC3 in IMR-32 cells that were transfected with BFP-Nedd8. [LC3 puncta formation in control vs. Nedd8-BFP overexpression: $p < 0.001$, $n = 71$]

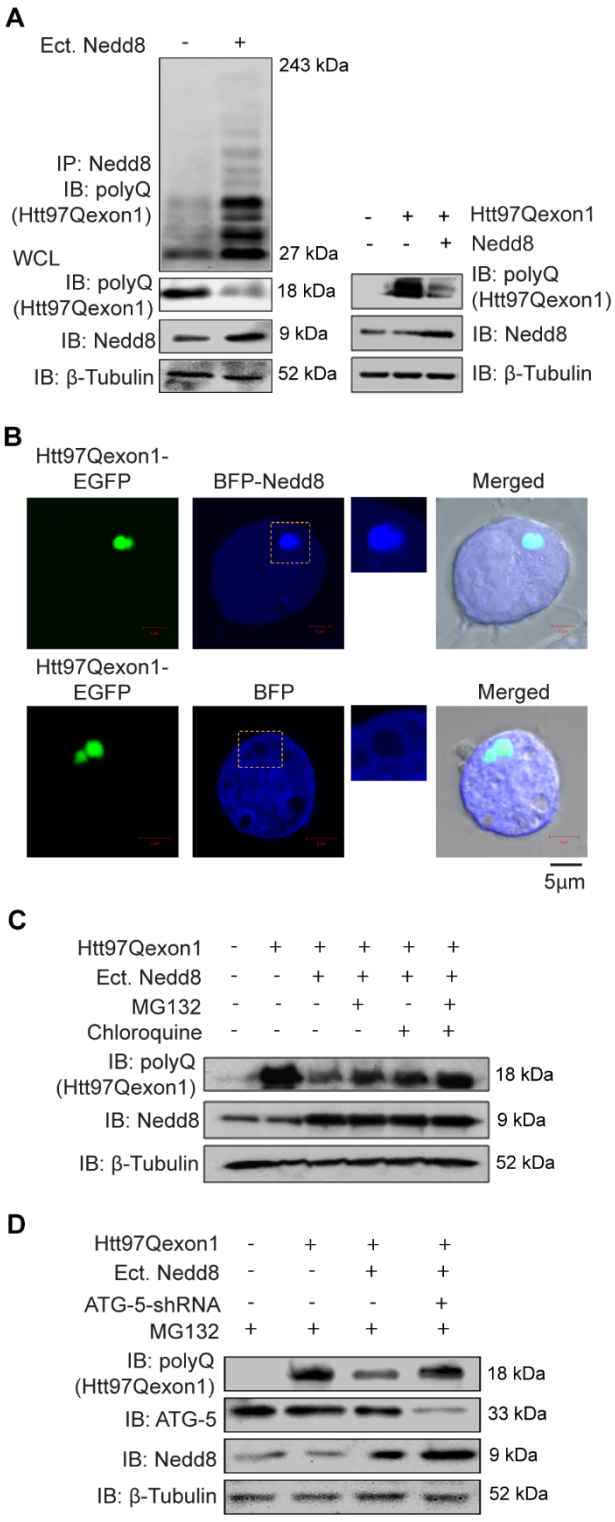

Figure 7. Huntingtin exon1 undergoes poly-neddylation. Poly-neddylated huntingtin exon1 is degraded by autophagy in IMR-32 cells. (A) [Left] Immunoblotting of immunecomplexes of Nedd8 [IP: Nedd8] with indicated antibodies for Htt97Qexon1, Nedd8 and β-tubulin from the lysate of IMR-32 cells that were transfected with either Htt97Qexon1 or Htt97Qexon1+Nedd8. Immunoprecipitation was done

in denaturing condition [WCL is whole cell lysate]. [Right] Immunoblotting for Htt97Qexon1, Nedd8 and β-tubulin with indicated antibodies from lysate of IMR-32 cells that were untransfected or transfected with Htt97Qexon1 and Nedd8. (B) Representative confocal microscopy images of colocalization of BFP-Nedd8, but not the BFP, with Htt97Qexon1-GFP in IMR-32 cells. (C) Immunoblotting for Htt97Qexon1, Nedd8 and β-tubulin with indicated antibodies from lysate of IMR-32 cells that were untransfected or transfected with Htt97Qexon1 and Nedd8 in presence of 20nM MG132 and/or 20nM chloroquine for 36 hours. (D) Immunoblotting for Htt97Qexon1, ATG-5, Nedd8 and β-tubulin with indicated antibodies from lysate of IMR-32 cells that were untransfected or transfected with Htt97Qexon1, ATG-5-shRNA and control [GFP]-shRNA in presence of 20nm MG132 for 36 hours.

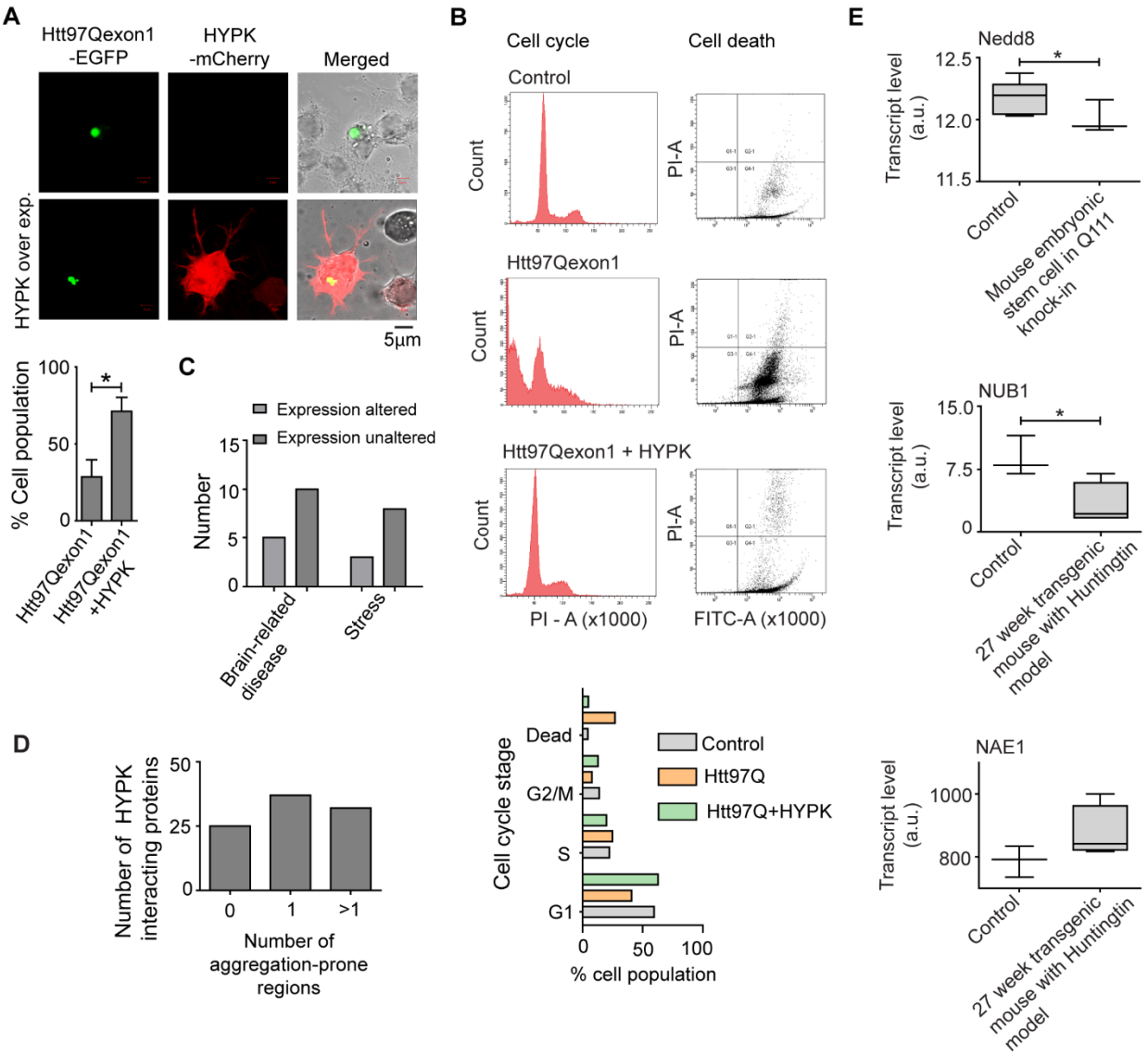

Figure 8. HYPK reduces proteotoxic stress and helps in cell survival. (A) Confocal microscopy images of differential neurite formation in Neuro2a cells that were transfected with Htt97Qexon1-GFP and HYPK-mCherry. [*Neurite formation in Htt97Qexon1-GFP vs. Htt97Qexon1-GFP+HYPK expressing cells: $p < 0.005$, $n = 112$]. (B) Representative FACS studies for cell cycle and cell death analysis of IMR-32 cells that were untransfected or transfected with Htt97Qexon1 and HYPK. [Upper left] Cell cycle stage analysis. [Upper right] Apoptotic cell death analysis. [Lower] Quantitative estimation of cell-cycle stages during different Htt97Qexon1 and HYPK expressing conditions. (C) GEO profile-based comparison of HYPK expression in different neurodegenerative diseases/ brain-related diseases and stressful conditions. (D) Number of HYPK interacting proteins according to presence of aggregation-prone regions in their sequences. (E) GEO profile-based analysis of transcript levels of Nedd8, NUB1, and NAE1 in Huntington's disease mouse models and control. [*Nedd8 transcript in control vs. embryonic stem cell of HD mouse: $p < 0.001$, $n = 6$; *NUB1 level in control vs. 27-week transgenic HD mouse: $p < 0.001$, $n = 6$].

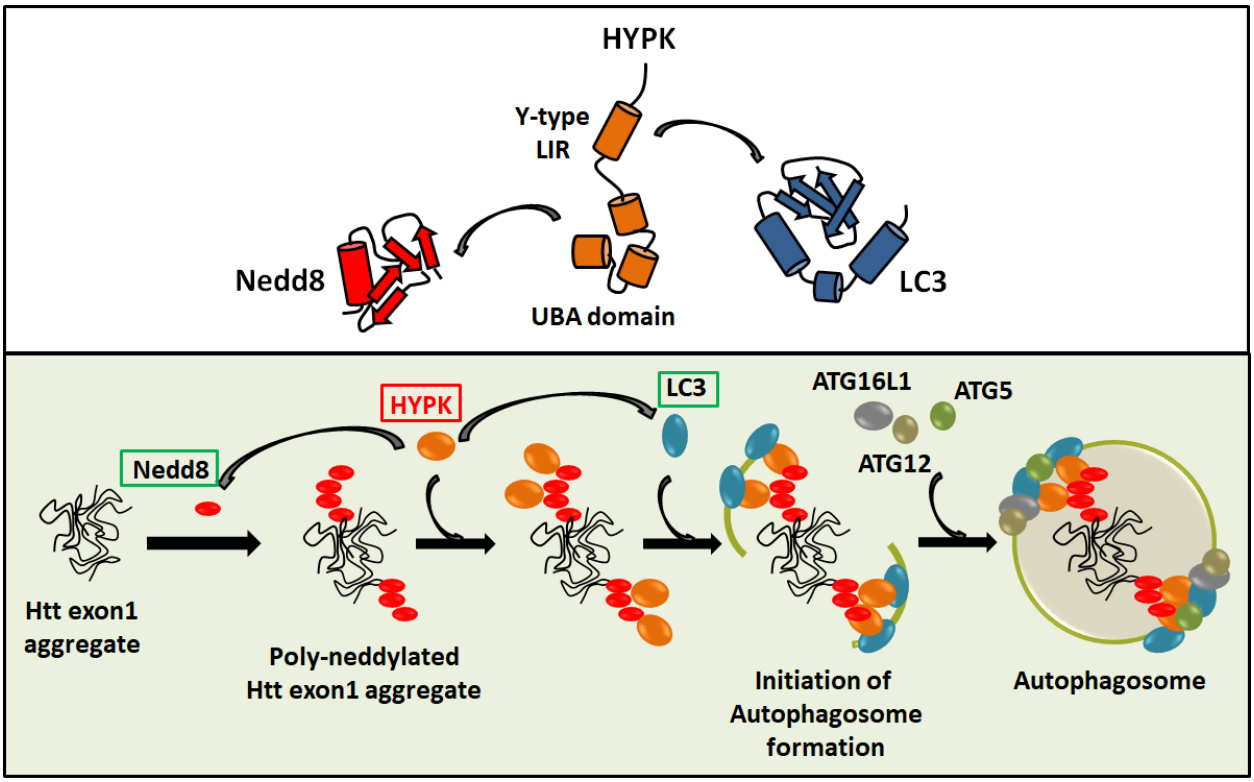

Figure 10. Model of HYPK mediated aggrephagy of poly-neddylated huntingtin exon1. HYPK functions as a scaffolding protein by simultaneously interacting with Nedd8 and LC3 by its UBA domain and Y-type LIR respectively. HYPK binds to the Nedd8 of poly-neddylated huntingtin exon1 aggregates, and subsequently attracts LC3 to the aggregates, thereby inducing the formation of autophagosome around the poly-neddylated huntingtin exon1 aggregates.

SUPPORTING FIGURES

A

```
C.elegans     (Nematoda)          ---INIKKEDLQLIMNELELQEGTVRAKLIETNGDVREALRSLC
Schistosoma   (Platyhelminthis)   ---IKVKNEDVSLICQELEVSKLTAERHLKEHQGNVFETLVALC
Trichinella   (Nematoda)          ---IVIKKEDVELLINEMELTKCTAEKTLRKYQGDVKKALIAML
Zea           (Angiosperm)        ---VKINPADVEIIASELELDKKIAERTLREHKGDAVAAVRFLL
Drosophila    (Arthropoda)        ---VQVKKEDIELIMNELLVSKAHAEKVLREQSGDVVAALEAII
Crassostrea   (Mollusca)          ---VKINKEDVDLIVAEMEITRQIAERTLREHNGDVVEALVALT
Xenopus       (Amphibia)          LAKVTIKKEDVELIMNEMEIPRSAAERSLREHMGNVVEALIALT
Danio         (Chondrichthyes)    LAKVTIKKEDVELIMGEMEISRAVAERSLREHMGNVVEALIALT
Human         (Mammalia)          ---VTIKKEDLELIMTEMEISRAAAERSLREHMGNVVEALIALT
Mouse         (Mammalia)          ---VTIKKEDLELIMTEMEISRAAAERSLREHMGNVVEALIALT
Gallus        (Aves)              LAKVTIKKEDLELIMNEMEISRAAAERSLREHMGNVVEALITLT
                                     : ::  *:.::  *: : .  ..  * :  *:.  ::  :
```

B

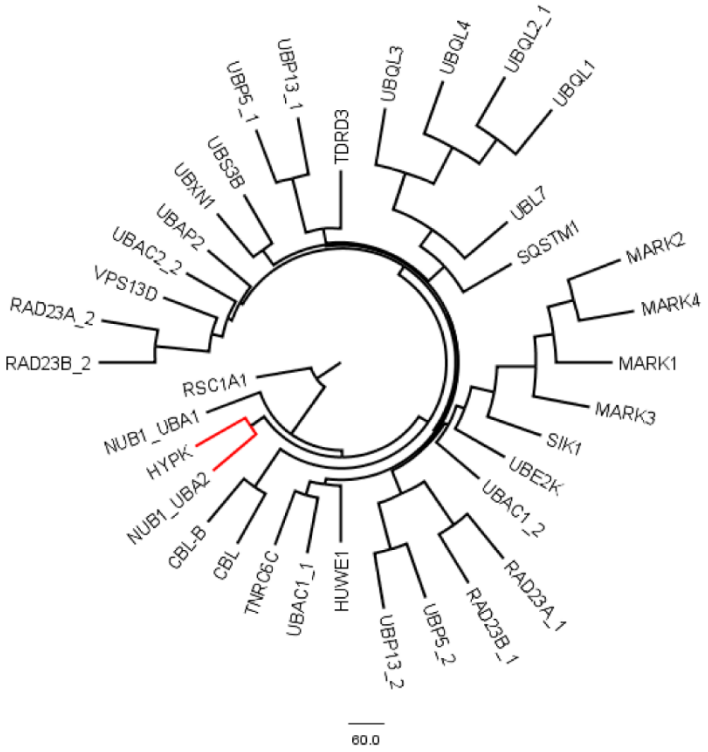

Supporting figure 1. The conserved UBA domain of HYPK is similar to the second UBA domain of NUB1 protein. (A) Multiple sequence alignment of the UBA domains of HYPK proteins of different organisms. (B) Cladogram representing the clustered UBA domains of different human proteins.

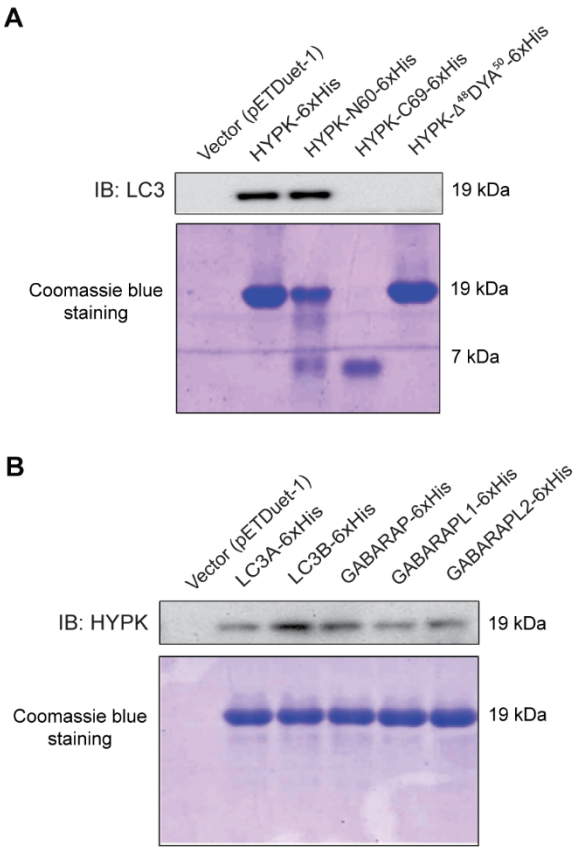

Supporting figure 2. The LC3-family proteins interact with the N-terminal region of HYPK. (A) Interaction of untagged recombinant LC3 with 6xHistidine tagged recombinant HYPK, HYPK-N60, HYPK-C69, HYPK-Δ^{48}DYA^{50} that were coexpressed in BL21DE3 strain of *Escherichia coli* by pETDuet-1 vector. [Upper] Immunoblot of LC3. [Lower] Coomassie blue staining of interacting pairs. (B) Protein-protein interactions of untagged HYPK with 6xHistidine tagged LC3A, LC3B, GABARAP, GABARAPL1, GABARAPL2 that were coexpressed in BL21DE3 strain of *Escherichia coli* by pETDuet-1 vector. [Upper] Immunoblot of HYPK. [Lower] Coomassie blue staining of interacting pairs. In both the experiments, empty vector is used for negative control.

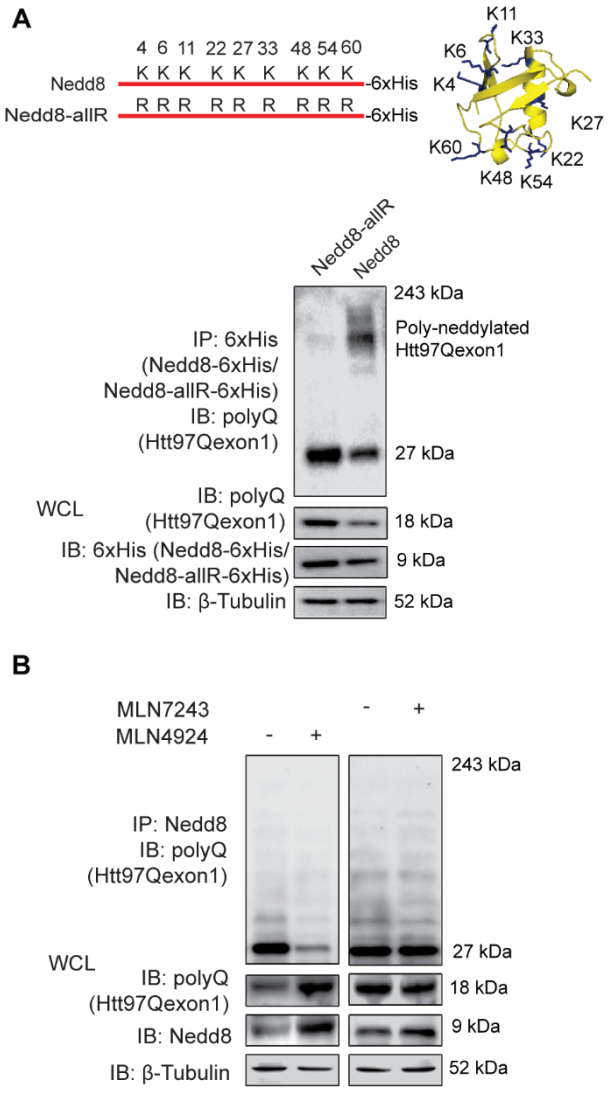

Supporting figure 3. Htt97Qexon1 undergoes poly-neddylation. The poly-neddylation chain linked to huntingtin exon1 in not contaminated with ubiquitin. (A) [Upper] Schematic representation of the Nedd8 constructs. [Lower] Immunoblotting of immunecomplex of 6xHis-Nedd8 (IP: 6xHis) and 6xHis-Nedd8-allR (IP: 6xHis) for Htt97Qexon1, Nedd8/Nedd8-allR and β-tubulin with indicated antibodies from lysate of IMR-32 cells that were transfected with 6xHis-Nedd8 and 6xHis-Nedd8-allR [WCL is whole cell lysate]. (B) Immunoblotting of immunecomplexes of Nedd8 (IP: Nedd8) for Htt97Qexon1, Nedd8, β-tubulin with indicated antibodies from lysate of IMR-32 cells that were transfected with Htt97Qexon1 in presence of 20nM MLN4924 or MLN7243 for 36 hours.

SUPPORTING INFORMATION

Supporting table 1. HYPK transcript expression level in neurodegenerative diseases and brain-related diseases.

Serial number	Disease / Disease model	GEO number	HYPK expression altered	HYPK expression unaltered	Remarks
1	Parkinson's disease: substantia nigra	GDS2821	-	Yes	-
2	X-linked recessive dystonia-parkinsonism	GDS1912	-	Yes	-
3	Alzheimer's disease: neurofibrillary tangles	GDS2795	-	Yes	-
4	HdhQ111 knock-in model of Huntington's disease: striatum	GDS4534	-	Yes	-
5	Amyotrophic lateral sclerosis model	GDS3408	-	Yes	-
6	Frontotemporal lobar degeneration with ubiquitinated inclusions and progranulin mutations: various brain regions - TDP-43	GDS3459	Yes	-	Downregulated
7	Amyloid Precursor Protein APP family members: adult prefrontal cortex	GDS4414	Yes	-	Upregulated
8	Spinocerebellar ataxia type 7 knock-in model: cerebellum - Spinocerebellar ataxia	GDS3545	-	Yes	-
9	Spinocerebellar ataxia type 1 knock-in model: cerebellum	GDS3544	-	Yes	-
10	Multiple sclerosis: brain lesions	GDS4218	Yes	-	Downregulated
11	Down syndrome: brain	GDS2941	Yes	-	Downregulated
12	Cerebellar cortex in schizophrenia	GDS1917	-	Yes	-
13	Measles virus brain infection model: right cerebral hemisphere	GDS4553	Yes	-	Upregulated
14	Simian immunodeficiency virus encephalitis model of HIV-associated dementia: hippocampus - Dementia	GDS4214	-	Yes	-

15	Progressive diabetic neuropathy: sural nerve	GDS4012	-	Yes	-

Supporting table 2. Expression level of HYPK transcript in different stressful conditions.

Serial number	Stress	GEO number	HYPK expression altered	HYPK expression unaltered	Remarks
1	Oxidative-stress induced neurodegeneration in Harlequin mutant: olfactory epithelium	GDS3365	-	Yes	-
2	Chronic stress effect on peripheral blood monocytes	GDS3383	-	Yes	-
3	Chronic endoplasmic reticulum stress imposed by misfolded surfactant protein C (HG-U133B)	GDS2054	-	Yes	-
4	Umbilical vein endothelial cell response to shear stress	GDS1317	-	Yes	-
5	Long-term heat-stress effect on skeletal muscle	GDS4104	Yes	-	Downregulated
6	Hypothalamus response to lipopolysaccharide	GDS324	-	Yes	-
7	Mechanical stress effect on fibroblasts	GDS1500	-	Yes	-
8	Chronic stress effect on the amygdala and hippocampus	GDS1794	-	Yes	-
9	Acute cold exposure effect on skeletal muscle	GDS4849	-	Yes	-
10	Sepsis effect on the skeletal muscle	GDS3463	Yes	-	Downregulated
11	Liver response to fasting	GDS3135	Yes	-	Upregulated